Science of the Total Environment 640–641 (2018) 1187–1204

Contents lists available at ScienceDirect

Science of the Total Environment

journal homepage: www.elsevier.com/locate/scitotenv

Implications of RCP emissions on future concentration and direct radiative forcing of secondary organic aerosol over China

Yu Zhang [a,b], Hong Liao [c,*], Xiang Ding [d], Duseong Jo [e,f], Ke Li [g]

[a] State Key Laboratory of Atmospheric Boundary Layer Physics and Atmospheric Chemistry (LAPC), Institute of Atmospheric Physics, Chinese Academy of Sciences, Beijing 100029, China
[b] University of Chinese Academy of Sciences, Beijing 100049, China
[c] Jiangsu Key Laboratory of Atmospheric Environment Monitoring and Pollution Control, Collaborative Innovation Center of Atmospheric Environment and Equipment Technology, School of Environmental Science and Engineering, Nanjing University of Information Science & Technology, Nanjing 210044, China
[d] State Key Laboratory of Organic Geochemistry and Guangdong Provincial Key Laboratory of Environmental Protection and Resources Utilization, Guangzhou Institute of Geochemistry, Chinese Academy of Sciences, Guangzhou 510640, China
[e] Cooperative Institute for Research in Environmental Sciences, University of Colorado at Boulder, Boulder, CO 80309, USA
[f] Department of Chemistry and Biochemistry, University of Colorado at Boulder, Boulder, CO 80309, USA
[g] John A. Paulson School of Engineering and Applied Sciences, Harvard University, Cambridge, MA 02138, USA

HIGHLIGHTS

- We examine future level and DRF of SOA in China driven by anthropogenic emissions.
- The ratio of SOA to $PM_{2.5}$ increases in 2010–2050 under RCP2.6, RCP4.5, and RCP8.5.
- SOA can exceed sulfate, ammonium, and BC in concentration in the future.

GRAPHICAL ABSTRACT

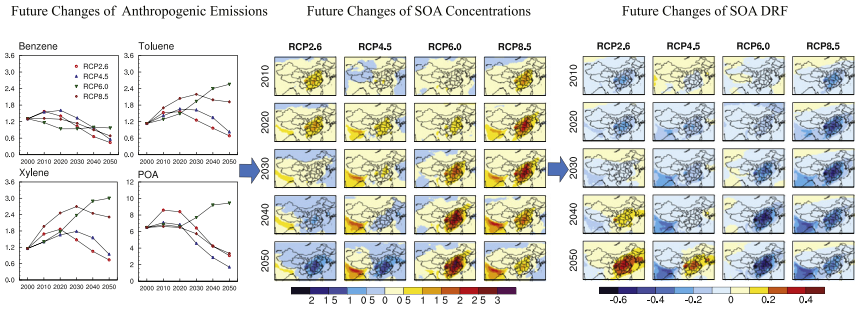

ARTICLE INFO

Article history:
Received 16 March 2018
Received in revised form 6 May 2018
Accepted 22 May 2018
Available online xxxx

Editor: P. Kassomenos

Keywords:
SOA
RCP
Anthropogenic emission
Contribution
DRF

ABSTRACT

This study applies the nested-grid version of Goddard Earth Observing System (GEOS) chemical transport model (GEOS-Chem) to examine future changes (2000–2050) in SOA concentration and associated direct radiative forcing (DRF) over China under the Representative Concentration Pathways (RCPs). The projected changes in SOA concentrations over 2010–2050 generally follow future changes in emissions of toluene and xylene. On an annual mean basis, the largest increase in SOA over eastern China is simulated to be 25.1% in 2020 under RCP2.6, 20.4% in 2020 under RCP4.5, 56.3% in 2050 under RCP6.0, and 44.6% in 2030 under RCP8.5. The role of SOA in $PM_{2.5}$ increases with each decade in 2010–2050 under RCP2.6, RCP4.5, and RCP8.5, with a maximum ratio of concentration of SOA to that of $PM_{2.5}$ of 16.3% in 2050 under RCP4.5 as averaged over eastern China (20°–45°N, 100°–125°E). Concentrations of SOA are projected to be able to exceed those of sulfate, ammonium, and black carbon (BC) in the future. The future changes in SOA levels over eastern China are simulated to lead to domain-averaged (20°–45°N, 100°–125°E) DRFs of +0.19 W m^{-2}, +0.12 W m^{-2}, − 0.28 W m^{-2}, and −0.17 W m^{-2} in 2050 relative to 2000 under RCP2.6, RCP4.5, RCP6.0, and RCP8.5, respectively. Model results indicate that future changes in SOA owing to future changes in anthropogenic precursor emissions are important for future air quality planning and climate mitigation measures.

* Corresponding authors.
E-mail address: hongliao@nuist.edu.cn (H. Liao).

https://doi.org/10.1016/j.scitotenv.2018.05.274
0048-9697/

1. Introduction

Secondary organic aerosol (SOA) is an important secondary pollutant in the atmosphere that affects atmospheric visibility (Huang et al., 2014; Yang et al., 2012), human health (Gaschen et al., 2010; Mauderly and Chow, 2008; Rohr, 2013), and climate change (Intergovernmental Panel on Climate Change (IPCC), 2013; Lambe et al., 2013). Over China, with rapid industrialization and urbanization over the past years, concentrations of $PM_{2.5}$ (fine particulate matter with a diameter of 2.5 μm or less) are at considerably high levels (Cao et al., 2012; Wang et al., 2015; Zhang et al., 2012), and the contributions of SOA to $PM_{2.5}$ are large in present-day and future (Colette et al., 2013; Huang et al., 2014; Liao et al., 2007).

Precursors of SOA include anthropogenic and biogenic volatile organic compounds (VOCs). Aromatics species, such as benzene, toluene, and xylene, are the most important anthropogenic precursors, which mainly come from solvent usage, vehicle exhaust, and biomass burning (Zhang et al., 2013). Biogenic SOA precursors such as isoprene and monoterpenes are released by various types of vegetation (Fu and Liao, 2012). Early studies indicated that anthropogenic contributions to global SOA production and burden are about 10% (Henze et al., 2008; Tsigaridis and Kanakidou, 2003), which are much smaller compared with those from biogenic precursors. However, recent ambient observations suggested that SOA formation from anthropogenic sources is large and even exceeds that from biogenic sources (Ding et al., 2012; Stone et al., 2009; Zhang et al., 2013). Modeling studies, on the basis of field observations, have examined the reasons for the underestimation of anthropogenic SOA in air quality models. By comparing with the ambient measurements during the Asia-Pacific Economic Cooperation (APEC, October 14 to November 14, 2014, Beijing), Li et al. (2017) showed that aromatic VOCs emissions and SOA yields have low biases by using the Regional Atmospheric Modeling System and Models-3 Community Multi-scale Air Quality (RAMS-CMAQ) model. With both aromatic emissions and yield parameters elevated, simulated SOA concentrations increased by nearly 4 times and compensated for 23.5% of the underestimation in SOA mass. The lack of photochemical aging process of aromatic species in models would also lead to low bias of SOA (Farina et al., 2010; Jathar et al., 2011; Jo et al., 2013; Murphy and Pandis, 2009). By comparing SOA concentrations simulated with the volatility basis set (VBS) approach in the GEOS-Chem model with observations in Europe, the United States, and East Asia, Jo et al. (2013) suggested a large impact of chemical aging on global SOA budget; the consideration of chemical aging of anthropogenic SOA leads to better agreement with observations and a 53% increase in SOA production (from 26.0 to 39.9 Tg $year^{-1}$) for year 2009. Furthermore, the presence of anthropogenic pollutants can facilitate biogenic SOA yields (Spracklen et al., 2011), since the oxidized biogenic VOCs can be condensed to the pre-existing primary organic aerosol (POA) or acids to form SOA (Carlton et al., 2010; Henze et al., 2008; Hoyle et al., 2009; Weber et al., 2007). Controlling manmade emissions would lead to reduction in both biogenic and anthropogenic SOA (Hu et al., 2017). Therefore, the role of anthropogenic emissions in SOA formation should earn much attention.

Better understanding of future air quality and future climate change requires the estimation of future concentration and radiative forcing of SOA. The future changes of SOA are dependent on future changes in emissions, climate, and land use. Heald et al. (2008) reported by using a coupled global atmosphere-land model that, over 2000–2100 under the IPCC A1B scenario, the global SOA burden was projected to change by +26%, +7%, +6%, and −14%, owing to future changes in biogenic emissions, anthropogenic emissions, climate (through changing lifetime of pollutants, excluding the responses of biogenic emissions to temperature), and land use, respectively. SOA production in Asia was simulated to have large increases (78% in anthropogenic SOA and 29% in biogenic SOA) over 2000–2100 because of the large increases in anthropogenic emissions in aromatics in this region. G. Lin et al. (2016) used the Community Earth System Model (CESM) to estimate the effects of future changes in climate, emissions, and land use on SOA concentrations. Future climate change was found to be the main driver of future changes in SOA under RCP8.5, which would increase annual mean global SOA burden by 25% during 2000–2100. Conversely, changes in anthropogenic emissions (including SOA formation from the uptake of glyoxal, methylglyoxal, and isoprene epoxydiols) and land use were simulated to reduce global SOA burden by 2% and 14%, respectively. In summary, the impacts of emission, climate and land use on future SOA vary with different scenarios, time slices and regions. We emphasize the role of future changes in anthropogenic emissions in this study because of the projected large future changes in aromatic emissions (Heald et al., 2008).

Previous studies have reported the simulated SOA direct radiative effect (DRE, defined as the differences in radiative flux with and without the presence of SOA) and direct radiative forcing (DRF, defined as the differences in DRE with and without anthropogenic SOA). By using Oslo CTM2, an off-line aerosol chemistry transport model, Hoyle et al. (2009) reported that the increases in SOA burden from 0.33 to 0.50 Tg led to a DRF of −0.06 W m^{-2} from the preindustrial time (1750) to present-day (2004), when SOA partitions only to organic aerosol. When SOA partitions to both organic and sulfate aerosols, SOA was simulated to have a DRF of −0.09 W m^{-2} over 1750–2004. A similar magnitude of forcing was obtained by Myhre et al. (2013), who reported a mean SOA DRF of −0.06 W m^{-2} over 1850–2000 from 6 models in the AeroCom Phase II experiment. Lin et al. (2014) simulated by using the Integrated Massively Parallel Atmospheric Chemical Transport (IMPACT) model that the increase in SOA burden from 0.59 Tg in the preindustrial time to 0.99 Tg in present-day exerted a direct forcing ranging from −0.12 to −0.31 W m^{-2}.

Previous simulations of SOA over China were mainly focused on present-day SOA concentrations. There have been studies updating SOA modules to capture the current spatiotemporal distributions of SOA on a regional or national scale (Feng et al., 2016; Han et al., 2016), analyzing the relative contribution from biogenic and anthropogenic precursors (Han et al., 2016; Hu et al., 2017; Jiang et al., 2012), quantifying the local and distant source contributions to SOA pollution in a certain area (J. Lin et al., 2016), and evaluating the effects of changes in emission, climate, and land cover and land use (LCLU) on SOA in the past decades (Fu et al., 2016). Yin et al. (2015) estimated a SOA DRE of −1.12 W m^{-2} at the top of atmosphere (TOA) in July 2006 by using the Regional Climate Model system vision 4 (RegCM4). However, the projection of SOA in the future atmosphere over China is barely implemented, not to mention the associated radiative forcing due to the changes in SOA burden.

In this study, we simulate future changes in SOA levels and associated DRF over China under the Representative Concentration Pathways (RCPs) scenarios. We use the nested-grid version of the global chemical transport model (GEOS-Chem) with a high resolution of 0.5° × 0.667°, driven by GEOS-5 assimilated meteorology. The VBS approach and updated yield parameters are implemented in this model, and photochemical aging is accounted for to improve the performance of SOA (Section 2). Section 3 compares our model results with observations. Sections 4 and 5 present simulated oxidant concentrations and SOA concentrations in China under the RCPs scenarios, with special attention to the four heavily polluted regions, including Beijing-Tianjin-Hebei (BTH, 36°–41°N, 114°–120°E), Yangtze River Delta (YRD, 29.5°–32.5°N, 118°–122°E), Pearl River Delta (PRD, 21°–24°N, 112°–116°E), and Sichuan Basin (SCB, 28°–31.5°N, 102°–108°E). The future roles of SOA in $PM_{2.5}$ under RCPs are examined in Section 6. The future DRF of SOA over China is presented in Section 7.

2. Model description, datasets, and numerical experiments

2.1. GEOS-Chem model

The simulations of SOA are carried out using the nested-grid capability of the GEOS-Chem model (version 9-01-03; http://acmg.seas.harvard.edu/geos/) driven by GEOS-5 assimilated meteorological data from the NASA's Global Modeling and Assimilation Office (GMAO) for

year 2010. The model is nested over Asia (11°S–55°N, 70°–150°E), with a horizontal resolution of 0.5°(latitude) × 0.667°(longitude) and 47 vertical layers up to 0.01 hPa. Lateral boundary conditions are supported by the global GEOS-Chem simulation at a horizontal resolution of 4°-(latitude) × 5°(longitude) with the concentrations of tracers updated every 3 h (Chen et al., 2009).

The GEOS-Chem model includes coupled O_3-NO_x-hydrocarbon chemistry (Bey et al., 2001) and aerosols including sulfate (Park et al., 2004), nitrate (Pye et al., 2009), ammonium, organic carbon (OC) and black carbon (BC) (Park et al., 2003), soil dust (Fairlie et al., 2007), and sea salt (Alexander et al., 2005). For POA, two tracers, hydrophobic and hydrophilic POAs, are considered in the model. It is assumed that 50% of POAs emitted are hydrophobic (Park et al., 2003). The hydrophobic POA becomes hydrophilic with an e-folding time of 1.15 days (Cooke et al., 1999; Park et al., 2003). The organic matter to organic carbon ratio for POA is assumed to be 2.1 (Jo et al., 2013; Pye and Seinfeld, 2010).

SOA is simulated by VBS approach with aging process. The lumped scheme and updated yield parameters of semi-volatile species can be found in Jo et al. (2013). The model divides all the semi-volatile organics into 6 bins by volatility. Each VOC is oxidized by OH, O_3, and NO_3 to form semi-volatile species with yield parameters suggested by Farina et al. (2010). These gas-phase oxidized species are allocated into 4 bins by effective saturation concentration, $[C^*] = [1, 10, 100, 1000]\,\mu g\,m^{-3}$, which are then subject to gas-particle partition to form SOA. SOA formation depends on NO_x levels (Henze et al., 2008). The chemical aging enhances SOA formation by reducing saturation vapor pressure to the next lower bin during the oxidation of gas-phase semi-volatile species by OH, thus, leading to increases in SOA mass yields (Jathar et al., 2011). It should be noted that the aging is only applied to aromatic species, since previous studies indicated that the consideration of aging of biogenic SOA in models resulted in overestimation of SOA concentrations as compared with observations (Lane et al., 2008; Murphy and Pandis, 2009, 2010). Following Jo et al. (2013), we use the rate constant of 4×10^{-11} cm^3 $molecule^{-1}$ s^{-1} to calculate the amount of aged gas-phase aromatic SOA at every time step. It is assumed that all SOA particles in this model are soluble.

Wet deposition in the GEOS-Chem model follows the scheme described by Liu et al. (2001) and applies only to soluble aerosols and gases. This scheme accounts for scavenging in convective updrafts, rain-out, and washout (Mari et al., 2000). Dry deposition uses a standard resistance-in-series model that is dependent on local surface types and meteorological conditions, as described by Wesely (1989).

The all-sky aerosol DRE at the TOA was calculated via the Rapid Radiative Transfer Model for GCMs (RRTMG), which was implemented into GEOS-Chem model by Heald et al. (2014). RRTMG calculates long-wave (in 16 bands) and shortwave (in 14 bands) radiative fluxes using the correlated-k method, with wavelength covering from 230 nm through 56 μm. The DRE of a specific aerosol species is calculated as the change in radiative flux with and without the aerosol. SOA DRE is calculated by zeroing POA in the optics of total organic aerosol in RRTMG. The DRF of SOA is estimated by differentiating the DRE between the pre-industrial (1850) and the present day (2000–2050). The same meteorological fields of year 2010 are used for all the simulations. For pre-industrial times, we shut down all the anthropogenic emissions and set the global mean CH_4 concentration at the level of year 1850 (0.7 ppm).

2.2. Emissions

Global anthropogenic emissions of aerosols and their precursors (NO_x, carbon monoxide (CO), non-methane VOCs (NMVOCs), sulfur dioxide (SO_2), ammonia (NH_3), BC, and OC) for each decade over the years of 2000–2050 under the RCPs were obtained from the website http://www.iiasa.ac.at/web-apps/tnt/RcpDb and then interpolated into the grid cells of the GEOS-Chem model. The original RCP emissions have a horizontal resolution of 0.5°(latitude) × 0.5°(longitude). Emissions are from 10 anthropogenic sectors (transport, shipping, aviation, energy, industry, residential and commercial combustion, solvents, waste treatment and disposal, agriculture, and agricultural waste burning) and two biomass burning sectors (grassland fires and forest fires). Emissions from shipping, aviation, and biomass burning have monthly variations, while those from other sectors have only annual mean values. We obtained monthly scaling factors from the Emission Database for Global Atmospheric Research (EDGAR) for the project of the Hemispheric Transport of Air Pollution (HTAP) vision 2 for the year of 2010, and applied them to all anthropogenic emissions except for shipping and aviation for all years and all RCP scenarios. The rationality of the scaling was described in Li et al. (2016).

The future changes in anthropogenic emissions of SO_2, NO_x, NH_3, and BC in China over 2000–2050 under the RCPs were shown in Fig. S1. We emphasize here on anthropogenic emissions of aerosols and aerosol precursors that have effects on SOA. Fig. 1 shows the evolutions of annual emissions of benzene, toluene, xylene, and POA over China in 2000–2050 under the four RCPs. Anthropogenic emissions of toluene and xylene display a similar pattern over the period of 2000–2050, except that the peak values of xylene occur a decade behind those of toluene, emerging in 2020 (2030) under RCP2.6 (RCP4.5). Both species peak in 2030 under RCP8.5. The evolutions of these two aromatics agree with the changes of NMVOCs in Zhu and Liao (2016). Unlike toluene and xylene, the emission of benzene increases from 2000 to 2010 (or 2020), and then decreases sharply to 2050 under RCP2.6, RCP4.5, and RCP8.5. The temporal evolution of POA emission is consistent with Li et al. (2016); emission peaks in 2010, keeps relative high value in 2020, and then decreases significantly to 2050 under RCP2.6, RCP4.5, and RCP8.5.

Biogenic emissions of NMVOCs are calculated by the Model of Emissions of Gases and Aerosols from Nature (MEGAN) (Guenther et al., 2006), which are dependent on meteorological conditions, land cover and vegetation types (Wiedinmyer et al., 2006) in the model.

Under RCP2.6 (RCP4.5), emissions of benzene, toluene, xylene, and POA are projected to decrease by 66.2% (57.4%), 39.6% (27.2%), 36.3% (18.3%), and 52.3% (73.9%) from 2000 to 2050, respectively. Under RCP8.5, emissions of benzene, toluene, xylene, and POA in 2000–2050 change by −47.6%, +69.2%, +99.9%, and −47.9%, respectively. For RCP6.0, Chinese emissions increase continuously from 2000 to 2050 for all species except benzene, and emissions of toluene, xylene, and POA increase by 125.8%, 160.0%, and 45.7% by 2050, respectively.

2.3. Observations

SOA tracers were observed simultaneously at 10 sites in 6 regions (North, East, Southwest, South, Northwest, and Northeast) of China from October 2012 to September 2013. These Filter-based particle samples were analyzed using SOA-tracer method (Ding et al., 2014; Ding et al., 2016; Ding et al., 2012). The observed concentrations of SOA are provided by Dr. Ding (xiangd@gig.ac.cn) and his group.

2.4. Numerical simulations

We perform simulations of SOA with emissions in 2000–2050 under the four RCPs. Meteorological fields are fixed at the year of 2010 for all the simulations considering that 2010 has the most realist present-day meteorology among 2000–2050. Each of the simulations is carried out for 18 months with the first 6 months initialized for both the global (4° latitude × 5° longitude) simulations that provide boundary conditions and the nested grid (0.5° latitude × 0.667° longitude) simulations. Since the meteorological fields and hence the biogenic emissions are fixed at year 2010 in all simulations, future changes in SOA are mainly caused by the changes in anthropogenic emissions.

Sensitivity studies are carried out to separate the role of future changes in POA from that of future changes in aromatics under RCP4.5:

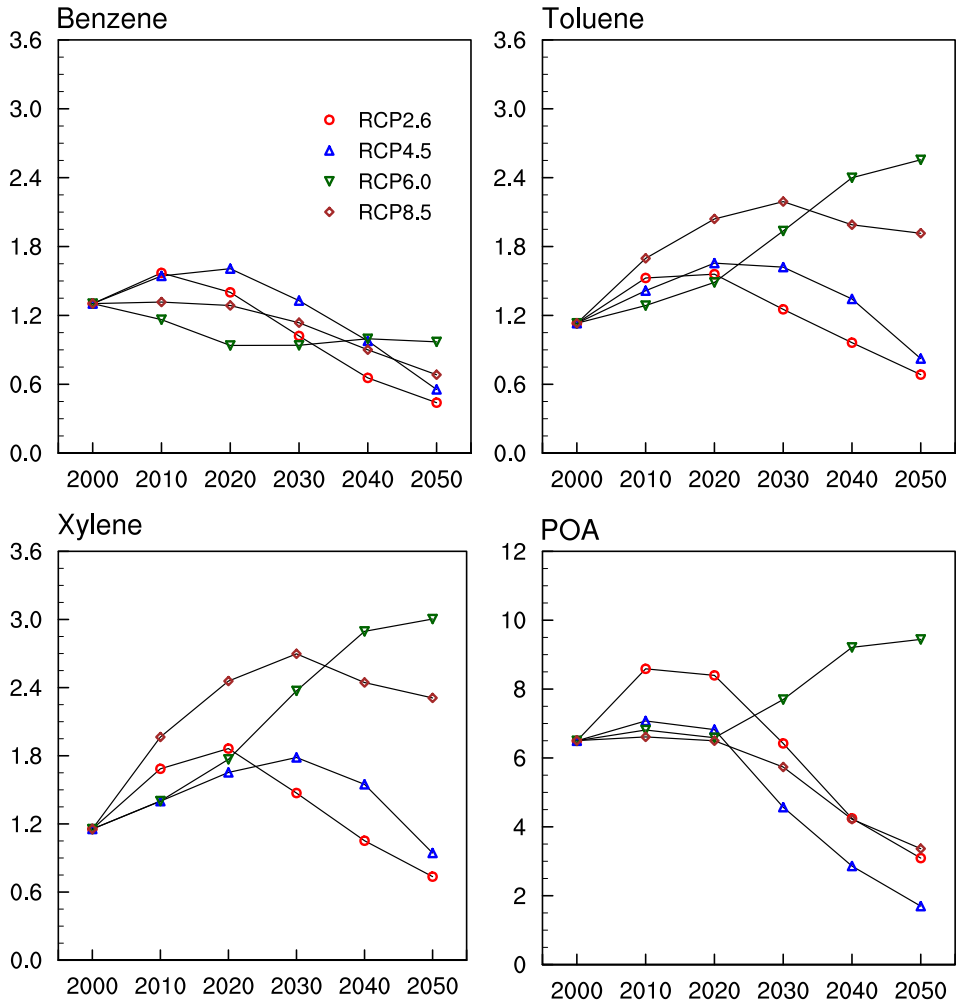

Fig. 1. Evolutions of annual anthropogenic emissions (units: Tg species year^{-1}) of benzene, toluene, xylene, and POA in China for the period of 2000–2050 under the four RCPs.

(1) CTRL_2010_RCP4.5: The control simulation with global anthropogenic emissions of aerosols and aerosol precursors at year 2010 levels under RCP4.5.
(2) POA_C2050: The same as the CTRL_2010_RCP4.5 simulation except that POA emissions in China are set to the year 2050 levels.
(3) Arom_C2050: The same as the CTRL_2010_RCP4.5 simulation except that aromatics emissions in China are set to the year 2050 levels.
(4) POA_Arom_C2050: The same as the CTRL_2010_RCP4.5 simulation except that the emissions of POA and aromatics in China are set to the year 2050 levels.

The impacts of 2010–2050 changes in POA, aromatics, and both of them in China on SOA formation can be quantified by (CTRL_2010_RCP4.5–POA_C2050), (CTRL_2010_RCP4.5–Arom_C2050), and (CTRL_2010_RCP4.5–POA_Arom_C2050), respectively.

3. Simulated present-day SOA concentrations over China and model evaluation

3.1. Seasonal mean surface-layer SOA concentrations

The simulated seasonal mean concentrations of SOA over China (Fig. 2) exhibit large temporal and spatial variability. The highest concentrations of about 5.50 μg m^{-3} are simulated over eastern China in JJA and SON, followed by the concentrations of about 5.00 μg m^{-3} in Sichuan Basin (SCB) in JJA and DJF. Such feature is in accord with other modeling studies, which indicated that the simulated highest SOA concentrations were in the range of 4 to 10 μg m^{-3} over 25°N–35°N of eastern China and SCB (Han et al., 2016; Hu et al., 2017; Jiang et al., 2012; J. Lin et al., 2016; Yin et al., 2015). Over Beijing-Tianjin-Hebei (BTH) area, SOA concentrations are about 4.50 μg m^{-3} in JJA and 2.50 μg m^{-3} in DJF. The simulated seasonal variation in BTH is in good agreement with the observed seasonality of SOA in Beijing reported by Lin et al. (2009). SOA in the Yangtz River Delta (YRD) is similar to that in BTH, both in magnitude and seasonal variability. The simulated highest SOA in JJA in these two regions can be explained by the strong photochemistry and high biogenic emissions. On the contrary, for the Pearl River Delta (PRD) in southern China, highest SOA exceeding 5.00 μg m^{-3} is found in SON, while relatively low level is simulated in JJA. This is because pollutants are diluted by the clean air from the oceans and washed out by precipitation during the East Asian summer monsoon (EASM) season (Zhao et al., 2010). Observations also showed that high SOA concentrations tend to occur in winter over PRD (Cao et al., 2003; Cao et al., 2004; Duan et al., 2007). Over western China, low SOA concentrations are simulated during all the seasons, which can be attributed to the uncertainty and incompleteness of emission inventory in this region, as indicated in other modeling studies (Fu et al., 2012; Yin et al., 2015).

3.2. Comparison of simulated SOA concentrations with measurements

Fig. 3 compares simulated monthly mean SOA concentrations with observed values at 10 sites as described in Section 2.3. Since the measurements were carried out over years 2012–2013, we show in Fig. 3

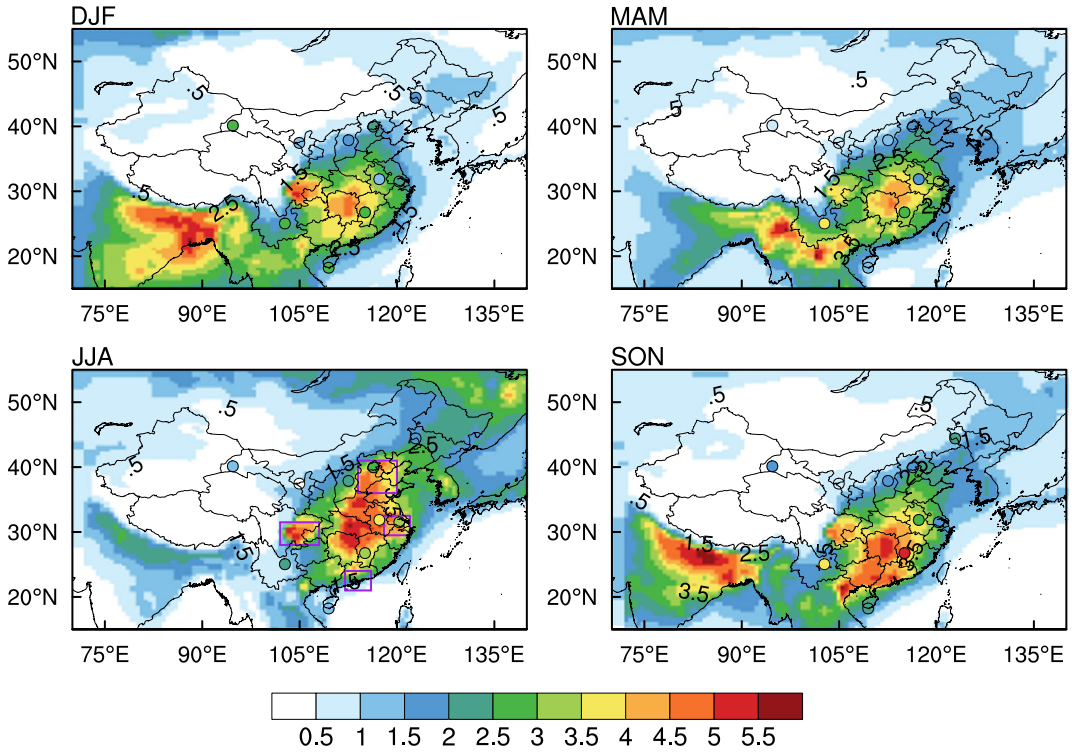

Fig. 2. Simulated seasonal mean surface-layer SOA concentrations (units: μg m^{-3}) for year 2010 under RCP4.5. The colored circles denote the observed seasonal mean concentrations of SOA at 10 sites over China measured by Ding's group. The purple rectangles in JJA denote the four polluted regions: Beijing-Tianjin-Hebei (BTH, 36°–41°N, 114°–120°E), Yangtze River Delta (YRD, 29.5°–32.5°N, 118°–122°E), Pearl River Delta (PRD, 21°–24°N, 112°–116°E), and Sichuan Basin (SCB, 28°–31.5°N, 102°–108°E). (For interpretation of the references to color in this figure legend, the reader is referred to the web version of this article.)

the simulated SOA concentrations with year 2010 and year 2020 anthropogenic emissions under RCP4.5. Simulated SOA concentrations at Taiyuan in northern China are in good agreement with observations, with mean bias (MB) of 0.07 μg m^{-3} and normal mean bias (NMB) of 3.9%. At Beijing, located in northern China, simulated SOA concentrations are high from April to October and low from November to next March. Our simulation in Beijing can generally capture the observed seasonal variation of SOA, except for a bit overestimation in June–July and underestimation in December–January. The observed monthly variations of SOA concentrations at Hefei, Wuxi, and Qianyanzhou (eastern China) are well reproduced except that the magnitude is overestimated in certain months. This overestimation is especially prominent in Hefei, where the observed SOA levels are about 1.00–2.00 μg m^{-3} in January–June while the simulated values are 3.00–4.50 μg m^{-3} during the same period. Model underestimation is found at the sites in southern China, with MB (NMB) of −1.66 μg m^{-3} (−50.6%) and − 0.73 μg m^{-3} (−39.1%) at Kunming and Sanya, respectively. At Dunhuang, the site in northwestern China, the simulated concentrations are too low to capture the features of the observed ones.

The scatterplot of simulated seasonal mean SOA concentrations versus observed values at 10 sites is shown in Fig. 4. Overall, the model underestimates seasonal SOA concentrations with MB of −0.19 μg m^{-3} and NMB of −8.7%. The correlation coefficient (R) of 0.62 indicates that the model can capture the spatiotemporal distribution of observed SOA concentrations in China to some extent. However, the model performance differs seasonally. Except for an overestimation in JJA, the model underestimates the observed SOA in other seasons. The MBs (NMBs) for DJF, MAM, JJA, and SON are −0.49 μg m^{-3} (−22.6%), −0.14 μg m^{-3} (−7.3%), 0.32 μg m^{-3} (14.2%), and − 0.46 μg m^{-3} (−19.0%), respectively. These biases can be attributed to the uncertainties in precursor emissions (Li et al., 2017; Fu et al., 2012) and yield parameters (Lane et al., 2008; Li et al., 2017), and the complex formation mechanism of SOA (Pye and Seinfeld, 2010; Fu et al., 2008; Lim et al., 2010).

4. Projected changes in surface-layer hydroxyl radical concentrations over China under the RCPs

It has been reported that gas-phase chemistry of aromatic hydrocarbons such as benzene, toluene and xylene is dominated by reaction with the hydroxyl radical (OH) (Calvert et al., 2002; Volkamer et al., 2002). OH is responsible for almost 100% of the oxidation of aromatics on an annual basis (Tsigaridis and Kanakidou, 2007). Relatively, reactions with other oxidants like ozone and NO_3 radicals as well as their photolysis are negligible (Volkamer et al., 2002). Therefore, before the presentation of the future concentrations of SOA, future changes in OH over China are examined. Previous studies (Su et al., 2012; Zhu and Liao, 2016) indicated that future increases in NO_x emissions result in the production of OH radicals, while future increases in emissions of NMVOCs, CO, and CH_4 lead to loss of OH.

Projected percentage changes in annual mean surface-layer OH concentrations in 2010–2050 for each decade relative to 2000 under RCPs are presented in Fig. 5. Under RCP2.6, OH concentrations increase over a large fraction of China by 2030 due to the increases in NO_x emissions and the decreases in CO and CH_4 levels (Fig. S1). Minor decreases of 10.0–20.0% are simulated over southern China in 2040–2050. Under RCP4.5, OH concentrations are simulated to increase slightly over China in 2010–2020, while widespread reductions are simulated in 2050 owing to the dominant role of NO_x reductions, with maximum decreases of exceeding 30.0% in southeastern China. For RCP6.0, large increases in NO_x emissions lead to overall increases in OH concentrations over China despite the decreases around BTH in all the years. Among the four RCPs, the largest increases in OH of exceeding 60.0% are simulated over southeastern China in 2010–2030 under RCP8.5, which can be attributed to the significant increases in NO_x emissions over this region during these years (Zhu and Liao, 2016). Without much NO_x emission in the west, the gradually high levels in CH_4 result in lower OH concentrations over western China in 2020–2050 under RCP8.5. The general distributions and magnitudes of OH changes over

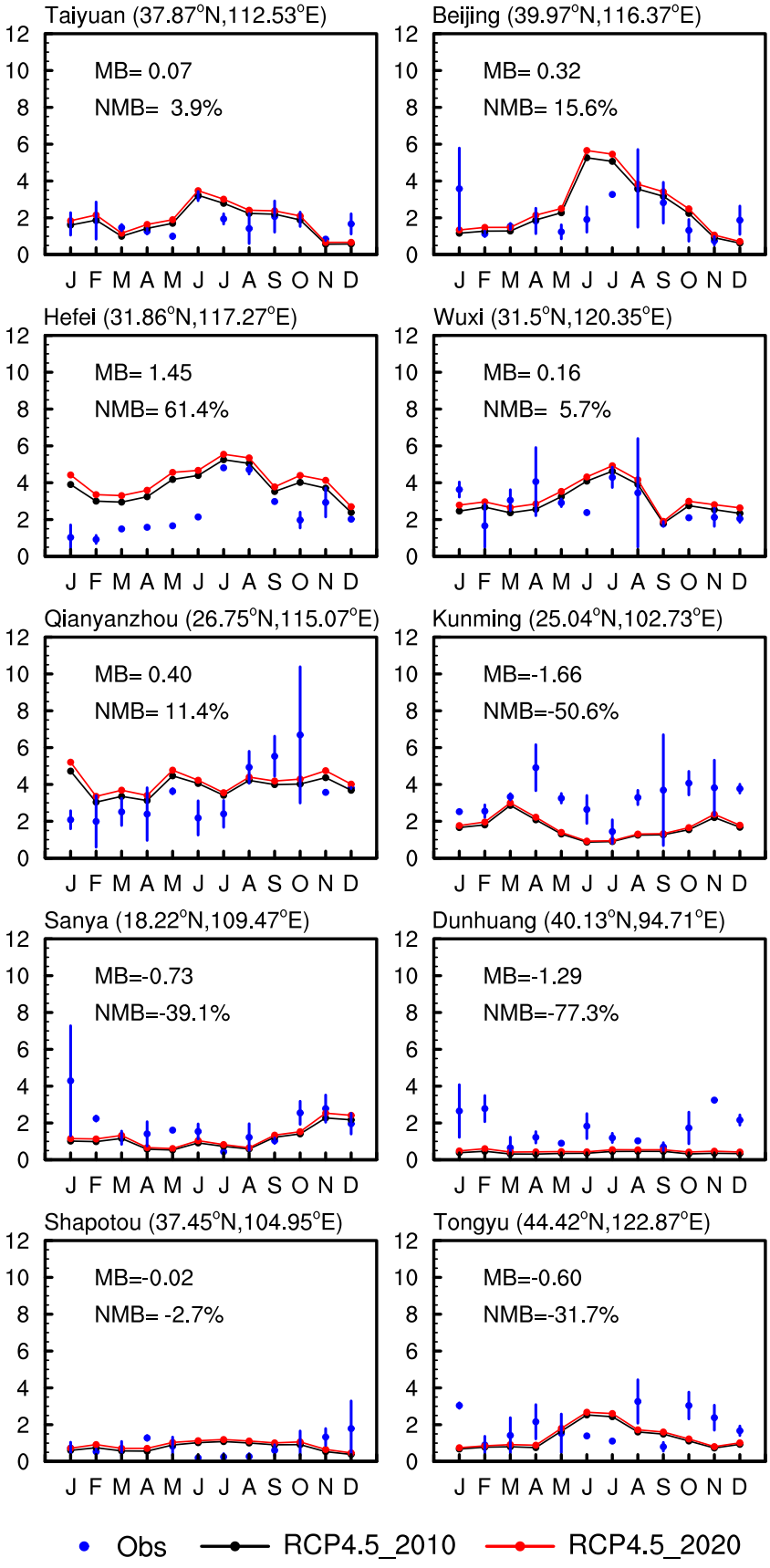

Fig. 3. Comparison of simulated monthly mean SOA concentrations (units: μg m^{-3}) in year 2010 (black lines) and year 2020 (red lines) under RCP4.5 with measurements (blue dots, thin blue vertical lines denote the standard deviations) at 10 sites. (For interpretation of the references to color in this figure legend, the reader is referred to the web version of this article.)

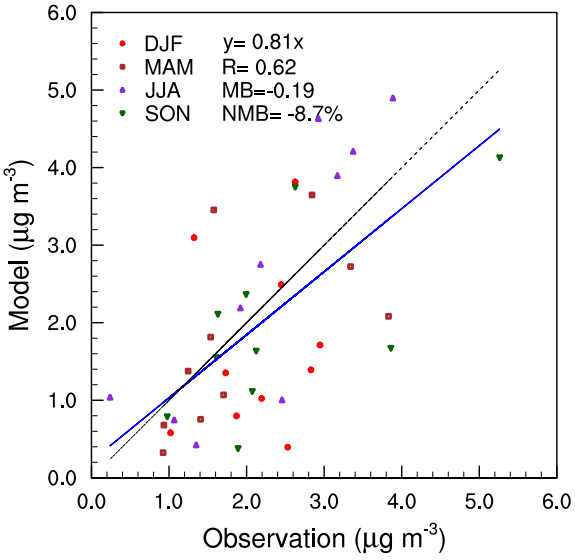

Fig. 4. Comparison of observed and simulated seasonal mean SOA concentrations (units: μg m^{-3}) at 10 sites. Also shown in plot are the 1:1 line (black dashed) and linear fit (solid blue line and equation), mean bias (MB, μg m^{-3}), normalized mean bias (NMB), and the correlation coefficient between observed and simulated concentrations (R). (For interpretation of the references to color in this figure legend, the reader is referred to the web version of this article.)

China during 2010–2050 relative to 2000 under the RCPs in this study are similar to those presented by Zhu and Liao (2016), who ran a full-chemistry simulation in 2000–2050 under the RCPs but excluded the formation of SOA. Compared with Zhu and Liao (2016), our study simulates a lower OH level in 2010–2050 over BTH, YRD, PRD, and SCB under all the RCPs (Fig. S3), because the emissions of aromatics are relatively large over these regions (Fig. S2) and the oxidation of aromatics consumes OH radicals (~0.4×10^6 molecules cm^{-3}) to form SOA, which was not considered in the former study.

5. Projected future SOA concentrations over China under the RCPs

5.1. Future changes in annual mean SOA concentrations

Fig. 6 shows the projected changes in annual mean surface-layer SOA concentrations for each decade relative to 2000 over China. Under RCP2.6, simulated SOA concentrations increase throughout China in 2010–2030. Maximum increases of 1.00–1.50 μg m^{-3} (~34.0%) are simulated in southern China and the SCB over 2010–2020. Reductions in surface-layer SOA concentrations are simulated over almost all parts of China in years of 2040 and 2050. Largest decreases of 1.50 μg m^{-3} (~35.0%) are simulated in 2050 over the same areas where SOA shows maximum increases during 2010–2030.

Under RCP4.5, the projected evolution and spatial distributions of SOA concentration are similar to those under RCP2.6. Annual mean surface-layer SOA concentrations exhibit increases over a large fraction

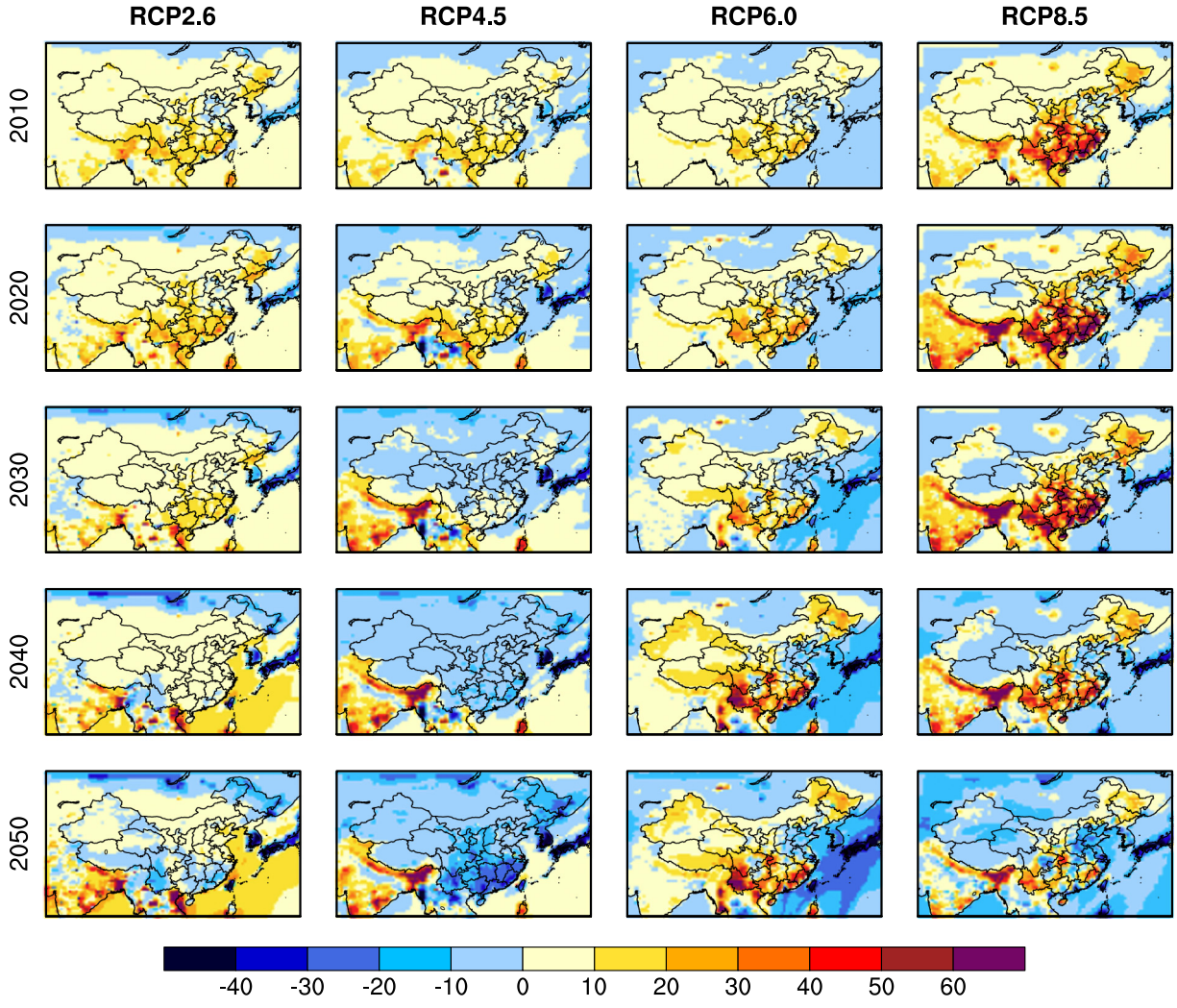

Fig. 5. Percentage changes in annual mean surface-layer OH concentrations (units: %) over 2010–2050 for each decade relative to 2000 under the four RCPs.

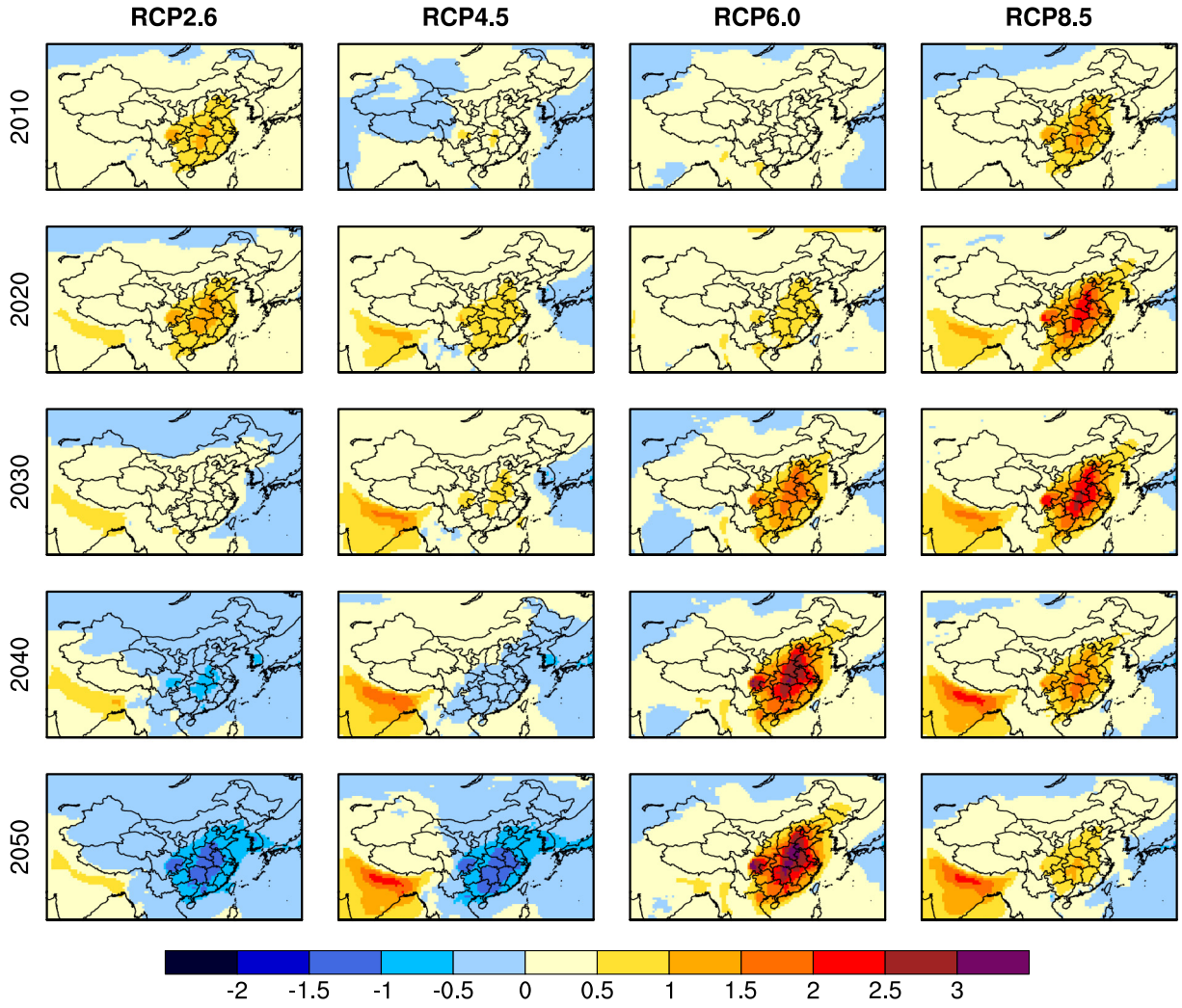

Fig. 6. Predicted changes in annual mean surface-layer SOA concentrations (units: μg m^{-3}) over 2010–2050 for each decade relative to 2000 under the four RCPs.

of China in 2010. The increasing trend is throughout China in 2020–2030, with the maximum increases of about 1.00 μg m^{-3} (~26.0%) over SCB in 2020. Concentrations of SOA are projected to decrease in 2040–2050; the maximum decreases of 1.50 μg m^{-3} (~33.0%) are simulated in southern China and the SCB by 2050.

For RCP6.0, the annual mean surface-layer SOA concentrations demonstrate a gradually rising trend in eastern China over 2000–2040 and then stabilize over 2040–2050. Relative to 2000, large increases of about 3.00 μg m^{-3} (~80.0%) are simulated to occur across Hunan, Hubei, and Henan provinces, as well as the SCB during 2040–2050.

The RCP8.5 leads to overall increases in annual mean SOA concentrations over China in all the simulated years, as a result of the increases in emissions of toluene and xylene over 2010–2050 relative to 2000. SOA concentrations reach peak values in 2030, with the maximum increases of 2.50–3.00 μg m^{-3} (~62.0%) in Hunan, Hubei, and Henan provinces. During 2040–2050, SOA concentrations show smaller increases of <2.00 μg m^{-3} (<40.0%) over these regions owing to the dominant role of reductions in toluene and xylene after 2030 (Fig. 1).

5.2. Future changes in seasonal mean SOA concentrations in the four heavily polluted regions

Fig. 7 shows the projected changes in seasonal mean surface-layer SOA concentrations averaged over the four heavily polluted regions, including BTH, YRD, PRD and SCB (domains are marked in Fig. 2). Note that the changes are calculated relative to year 2000. Fig. 8 shows the maximum percentage changes in seasonal mean SOA concentrations during 2010–2050 relative to 2000 and the years in which these maximums occur over these four regions.

Over the four regions, the surface-layer SOA concentrations exhibit similar trends in all seasons (Fig. 7), with peak values found in 2020 under RCP2.6 and RCP4.5, in 2050 under RCP6.0, and in 2030 under RCP8.5 (Fig. 8). The patterns of future changes in SOA concentrations mimic the future changes in annual emissions of toluene and xylene and do not follow those of benzene, which can be explained by two reasons. First, the future changes in emissions of toluene and xylene are larger than those of benzene, especially under RCP6.0 and RCP8.5 (Fig. 1). Second, according to chamber experiments, toluene and xylene have higher reaction rate constants than benzene (Calvert et al., 2002; Ng et al., 2007). The yield parameters of toluene and xylene in our model are set to be 1.08 and 1.16 times higher than the yield parameter of benzene (Jo et al., 2013), leading to the large impacts from toluene and xylene on future SOA formation.

5.2.1. BTH

The projected future increases in SOA concentration are the largest in JJA, followed by those in DJF, SON, and MAM (Fig. 7). The future increases in precursor emissions over BTH are the largest in DJF among all seasons. For example, in 2020 under RCP2.6, aromatics emission over BTH increases by 0.14 GgC $grid^{-1}$ $month^{-1}$ in DJF and by 0.11 GgC $grid^{-1}$ $month^{-1}$ in other seasons. Similarly, relative to 2000, the increase in POA emission in 2020 is larger in DJF than in other

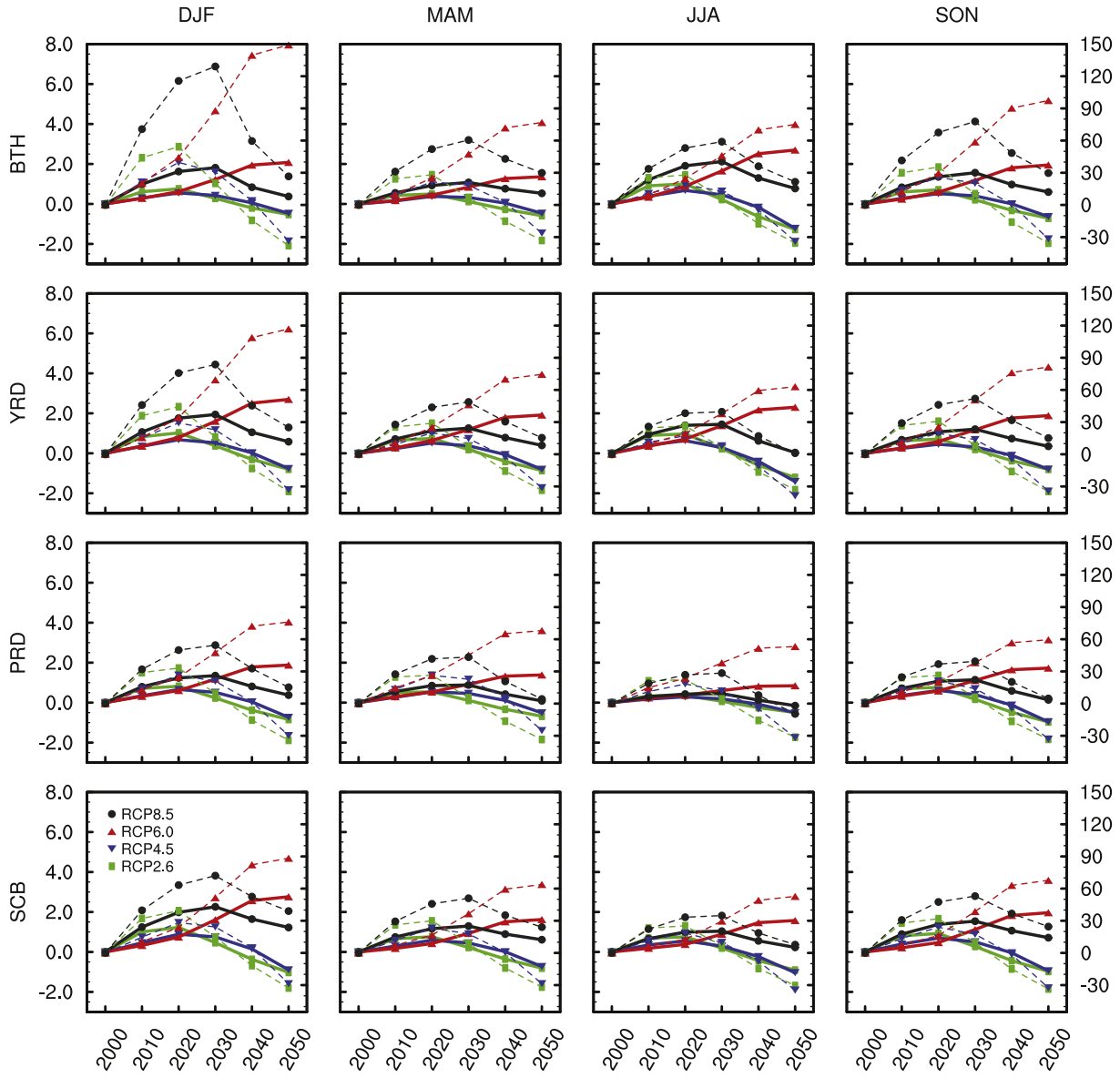

Fig. 7. Relative changes (left Y axis, solid lines, units: μg m^{-3}) and percentage changes (right Y axis, dashed lines, units: %) in seasonal mean surface-layer SOA concentrations over 2010–2050 for each decade relative to 2000 in the four polluted regions under the four RCPs.

seasons under RCP2.6. The simulated maximum increases in SOA concentration in JJA can be attributed to the strongest photochemical reactions.

Under RCP2.6, the largest increase of 1.00 μg m^{-3} (28.0%) in SOA concentration is simulated in JJA in 2020. The maximum for RCP4.5 is also found during this period, but with a relatively smaller magnitude of change of about 0.68 μg m^{-3} (+18.8%). Under RCP6.0, the largest increase by 2050 is 2.70 μg m^{-3} (75.0%) in JJA. For RCP8.5, the increases reach peak in JJA in 2030, with an increase of 2.10 μg m^{-3} (59.0%) in concentration. The largest decreases by 2050 are 1.28 μg m^{-3} (35.5%) and 1.22 μg m^{-3} (34.0%) in JJA under RCP2.6 and RCP4.5, respectively. There is no projected decrease relative to 2000 for RCP8.5, since the emissions of toluene and xylene in 2010–2050, despite the mitigation, are still higher than those in year 2000.

5.2.2. YRD

Over YRD, the simulated future increases in SOA have the largest values in DJF and the second largest values in JJA. The largest future increases in SOA are 1.02 μg m^{-3} (44.3%) in 2020, 0.67 μg m^{-3} (29.3%) in 2020, 2.70 μg m^{-3} (116.9%) in 2050, and 1.94 μg m^{-3} (83.7%) in 2030 under RCP2.6, RCP4.5, RCP6.0, and RCP8.5, respectively. The magnitudes of changes are about the same in MAM and SON. It should be noted that, in DJF and MAM, the future changes in SOA over YRD are slightly larger than those over BTH. This can be attributed to the slightly higher precursor emissions and lower latitudes (stronger photochemical reactions) of YRD.

5.2.3. PRD

Future changes in SOA in PRD are the lowest among the four polluted region in DJF, MAM, and JJA. Surface-layer SOA concentrations in DJF exhibit the largest increases of 0.90 μg m^{-3} (33.2%) in 2020, 0.69 μg m^{-3} (25.4%) in 2020, 2.06 μg m^{-3} (75.9%) in 2050, and 1.51 μg m^{-3} (55.5%) in 2030 under RCP2.6, RCP4.5, RCP6.0, and RCP8.5, respectively. Over PRD, future changes in SOA are the lowest in JJA among all the seasons, although the future changes of precursor emissions are not the smallest in JJA. For example, under RCP2.6 in 2020, the increase in POA emission over PRD is the largest in JJA and the increase in aromatics emission is the second largest in JJA just behind that in SON. The small changes of SOA concentration in JJA can be attributed to the rainfall associated with the EASM, which suppresses

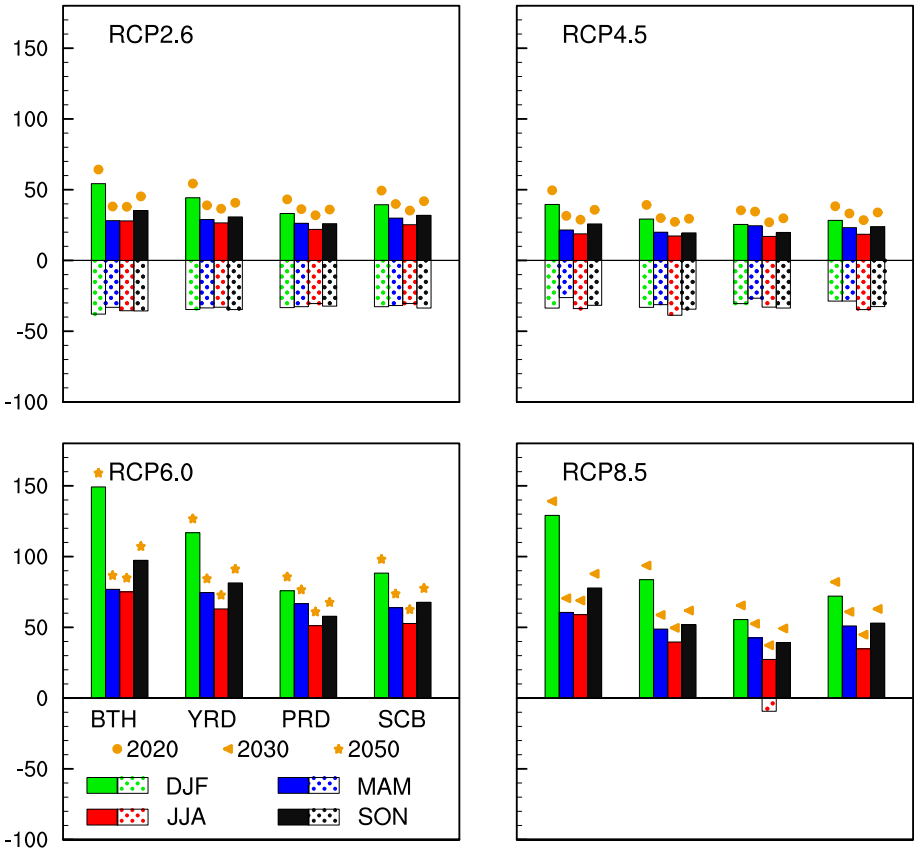

Fig. 8. The maximum percentage changes (units: %) of predicted seasonal mean SOA concentrations over 2010–2050 for each decade relative to 2000 in the four polluted regions under the four RCPs. The solid (dotted) bars denote the maximum percentage increase (decrease). The years in which the maximum increases occur are marked by orange symbols. For example, under RCP2.6 over BTH, the maximum percentage increase in DJF SOA occurs in 2020. Note that the maximum percentage decreases all occur in 2050, so we don't use symbols to mark them out.

photochemical production of pollutants over southern China (Zhao et al., 2010). On the contrast, relatively large changes in SOA are simulated in both DJF and SON. Note that the emissions of aromatics over PRD are about the same in the four seasons. The comparable large SOA changes in DJF and SON can be attributed to the warm weather due to the low latitudes.

5.2.4. SCB

Over SCB, the largest increases are simulated in DJF under all RCPs, with the maximums of 1.23 μg m^{-3} (+39.4%) in 2020, 0.89 μg m^{-3} (+28.3%) in 2020, 2.76 μg m^{-3} (+88.3%) in 2050, and 2.26 μg m^{-3} (+72.1%) in 2030 under RCP2.6, RCP4.5, RCP6.0, and RCP8.5, respectively. The largest decrease is simulated by 2050, with 1.02 μg m^{-3} (32.7%) in DJF and 1.04 μg m^{-3} (34.7%) in JJA under RCP2.6 and RCP4.5, respectively.

Note that the magnitude of future changes in emissions of aromatics in SCB is comparable to that in BTH (Fig. S2). For example, emissions of aromatics over SCB (BTH) increase by 0.14–0.24 GgC $grid^{-1}$ $month^{-1}$ (0.12–0.33 GgC $grid^{-1}$ $month^{-1}$) in DJF in 2020 under all RCPs except RCP6.0. However, the changes in SOA over SCB are larger than those over BTH in all seasons except JJA. The lower latitudes and the unique terrain of basin (not favorable for pollution diffusion) play an important role in SOA concentration over SCB.

6. The contribution of SOA to $PM_{2.5}$ over China under the RCPs

6.1. Annual mean contribution of SOA to $PM_{2.5}$

Fig. 9 shows the annual mean contribution of SOA to $PM_{2.5}$ over 2000–2050 under the four RCPs. $PM_{2.5}$ is the sum of sulfate, nitrate, ammonium, BC, POA, and SOA. The contribution of SOA to $PM_{2.5}$ is 12.6% averaged over the whole of China in 2010 under RCP4.5. High percentages are simulated over western China, with the maximums exceeding 24.0% in Kunming, Sichuan and Xizang provinces. The contributions over eastern China are relatively low with a domain-averaged (20°–45°N, 100°–125°E) value of 9.9%. The discrepancy between eastern and western China can be attributed to the different local $PM_{2.5}$ levels which are higher in the polluted eastern China than in the relatively clean western China. It should be noted that SOA is from both anthropogenic and biogenic sources. In years 2000–2050, biogenic SOA accounts for 36.0–46.7% of SOA and therefore contributes 4.0–7.3% to $PM_{2.5}$, as values are averaged over the whole of China.

Under all the RCPs (except RCP6.0), simulated SOA contribution to $PM_{2.5}$ increase gradually with decades. The percentages averaged over eastern China increase from 10.5%, 9.9%, and 11.1% in 2010 to 13.8%, 16.3%, and 15.3% in 2050 under RCP2.6, RCP4.5, and RCP8.5, respectively, indicating that SOA plays a more and more important role in the future. Under RCP6.0, however, the percentages barely change.

6.2. Projected contribution of SOA to $PM_{2.5}$ in the four heavily polluted regions

Fig. 10 shows the contributions of SOA to $PM_{2.5}$ over the four heavily polluted regions in DJF and JJA of 2000–2050 under the four RCPs. The contributions of SOA to $PM_{2.5}$ are 3.2–14.3% in DJF, and 10.0–27.0% in JJA over these four regions. The larger percentages in JJA can be attributed to the abundant photochemistry formation of SOA as well as the relatively low levels in $PM_{2.5}$ during summertime (Li et al., 2016). Fig. 11 shows the future changes in the concentrations of $PM_{2.5}$ components to see more clearly the future role of SOA.

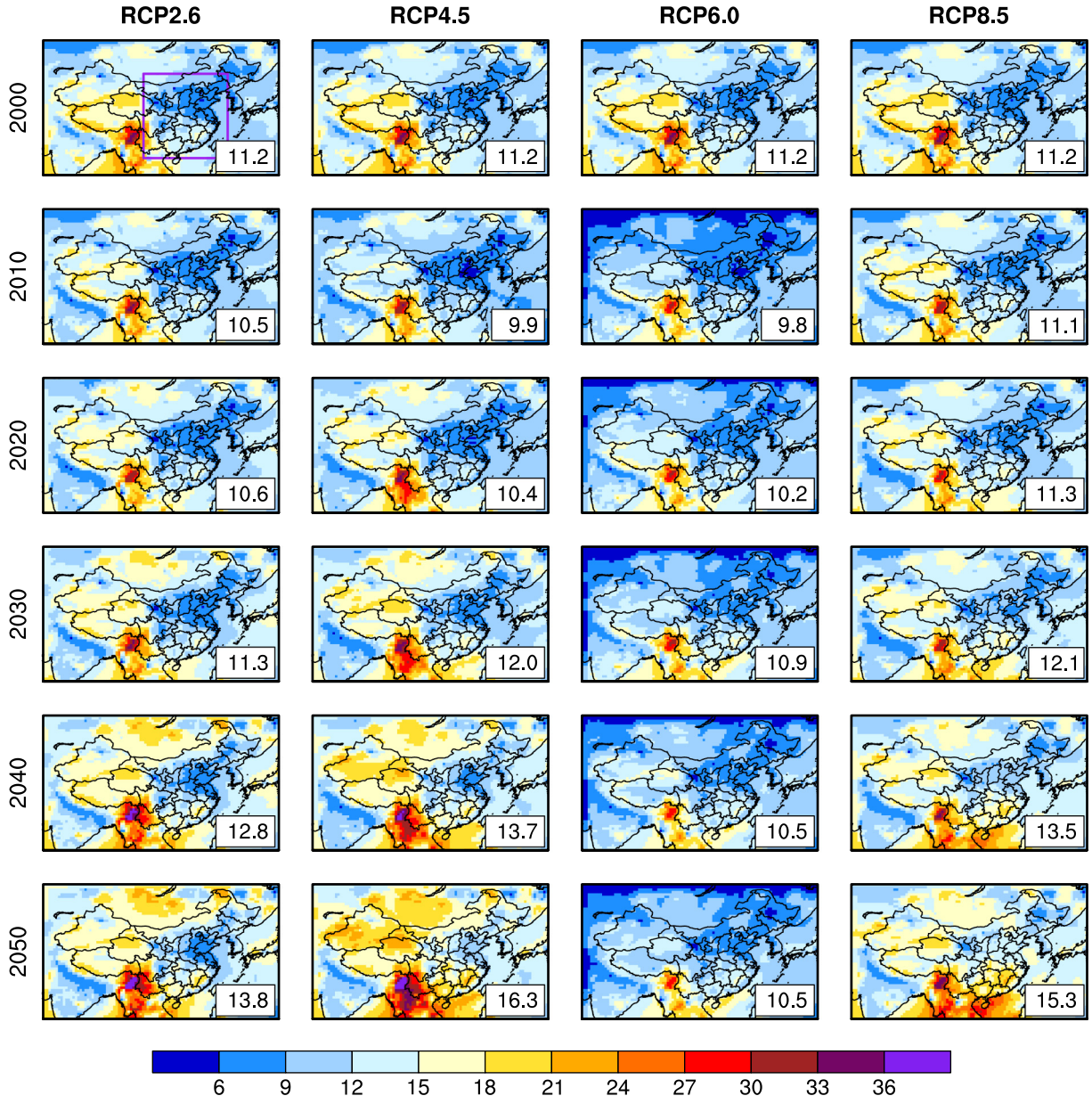

Fig. 9. The contribution of SOA to $PM_{2.5}$ (units: %) in China over 2000–2050 under the four RCPs. The percentages averaged over eastern China (20°–45°N, 100°–125°E; see the purple frame in the first panel) are shown in the bottom-right corner of each panel. (For interpretation of the references to color in this figure legend, the reader is referred to the web version of this article.)

Over BTH, the contribution of SOA to $PM_{2.5}$ in DJF is the least (about 3.0–6.0%) among all the aerosols in the present and future except that SOA concentration (1.67 μg m^{-3}) will overtake sulfate (1.37 μg m^{-3}) and BC (1.61 μg m^{-3}) in 2050 under RCP8.5. Wintertime $PM_{2.5}$ concentrations that meet First Grand National Standard (FGNS, annual $PM_{2.5}$ concentration below 35 μg m^{-3}) are predicted to occur in 2040 under RCP2.6 and RCP4.5, and in 2050 under RCP8.5. In JJA, concentrations of SOA (2.36–6.44 μg m^{-3}) exceed those of BC (0.67–3.19 μg m^{-3}) in all the years under all the RCPs. Moreover, SOA (2.36–5.00 μg m^{-3}) will overtake sulfate (1.93–4.16 μg m^{-3}) and ammonium (1.81–4.09 μg m^{-3}) in 2050 under RCP2.6 and RCP4.5, and in 2040 under RCP8.5. The years when summer $PM_{2.5}$ levels meet the FGNS occur in 2030 under RCP2.6 and RCP4.5, and in 2040 under RCP8.5.

Over YRD, the contributions of SOA to $PM_{2.5}$ in DJF (5.2–9.7%) are larger than those over BTH. SOA (1.52–3.33 μg m^{-3}) in DJF exceed BC (1.34–2.51 μg m^{-3}) in concentrations in 2050 under RCP2.6, and in 2040 under RCP8.5. In JJA, SOA (2.33–6.14 μg m^{-3}) exceeds BC (0.65–3.23 μg m^{-3}) in all the years under all the RCPs. The concentration of SOA also exceeds that of sulfate (ammonium) in JJA 2040 (2030) under RCP2.6 and RCP8.5, and in 2050 (2040) under RCP4.5. In consideration of the FGNS, $PM_{2.5}$ concentrations in JJA are expected to be controlled well for all the RCPs except RCP6.0. However, $PM_{2.5}$ levels in DJF reduce to <35 μg m^{-3} in 2040 under RCP4.5, and in 2050 under RCP2.6 and RCP8.5.

Over PRD, the contributions of SOA to $PM_{2.5}$ in DJF are highest among all the regions, with percentages above 8.9% for all the RCPs. SOA (2.03–5.12 μg m^{-3}) overtakes BC (1.01–4.74 μg m^{-3}) in concentrations after 2030 under all the RCPs. The wintertime $PM_{2.5}$ concentrations meet FGNS in 2040 under RCP2.6 and RCP8.5, and in 2030 under RCP4.5. In JJA, the concentration of SOA (1.66–3.73 μg m^{-3}) overtakes that of ammonium (0.97–3.20 μg m^{-3}) in all the years under all the RCPs. SOA overtakes BC (sulfate) in concentrations after 2030 (2040) under RCP2.6 and RCP8.5, and after 2030 (2050) under RCP4.5. Future $PM_{2.5}$ levels in JJA are all under the FGNS, which do not exceed 10.00

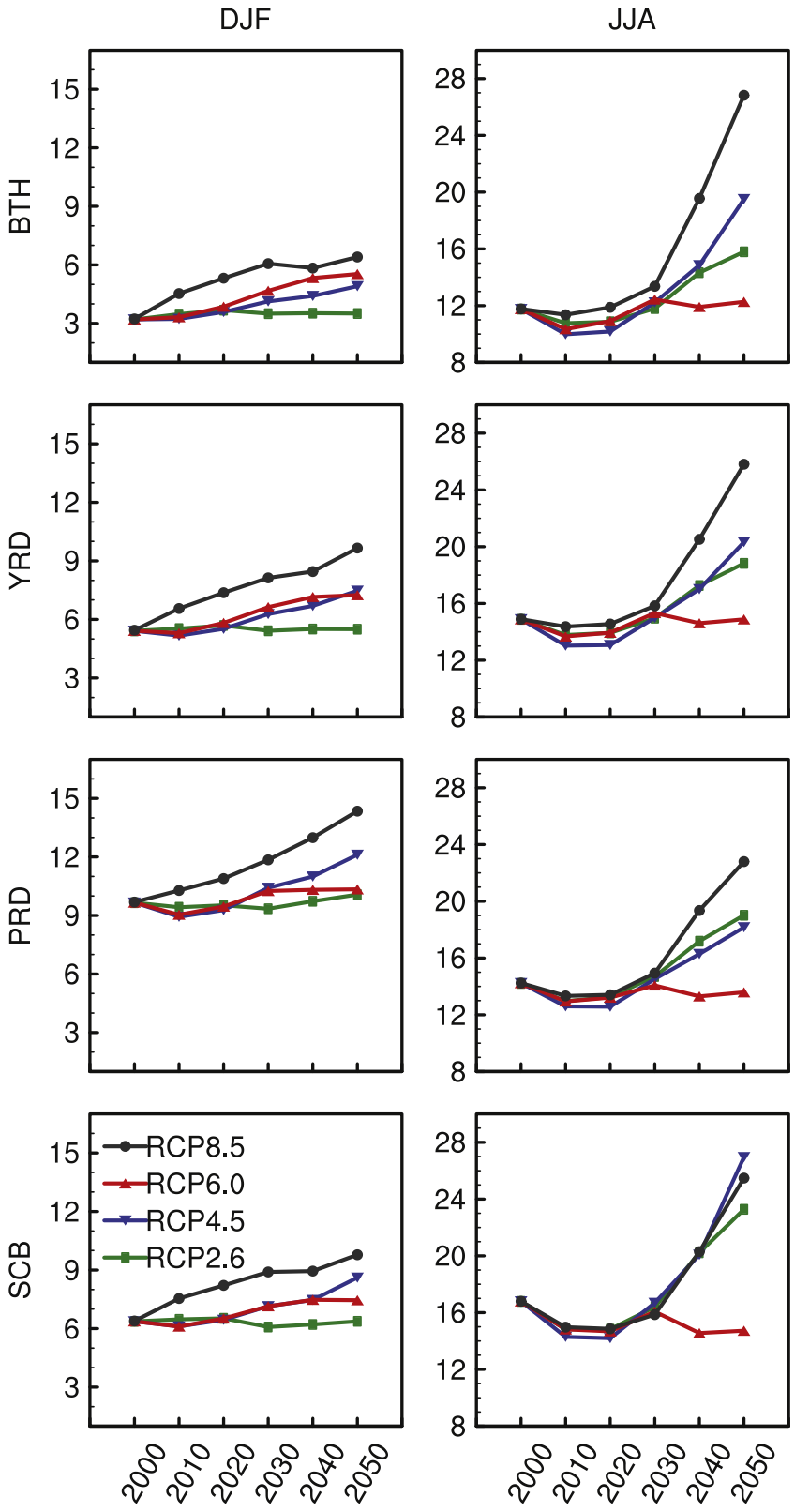

Fig. 10. Predicted 2000–2050 changes in the seasonal mean contribution of SOA to $PM_{2.5}$ (units: %) in DJF (left) and JJA (right) for the four polluted regions under the four RCPs.

μg m^{-3} in 2050 under all the RCPs except RCP6.0. Therefore, if the emissions in winter could be well constrained, PRD would be the most possible city that meets FGNS.

Over SCB, the concentration of SOA (2.08–4.64 μg m^{-3}) in DJF overtakes that of BC (1.53–3.32 μg m^{-3}) in 2040 under RCP2.6 and RCP8.5. In JJA, SOA exceeds BC under all the RCPs and ammonium under RCP2.6 during the period of 2000–2050. SOA also exceeds ammonium in JJA after 2030 under RCP4.5 and RCP8.5, and sulfate after 2040 under all the RCPs except RCP6.0. Although $PM_{2.5}$ in JJA is within FGNS, the control of $PM_{2.5}$ pollution in DJF is challenging over SCB. High $PM_{2.5}$

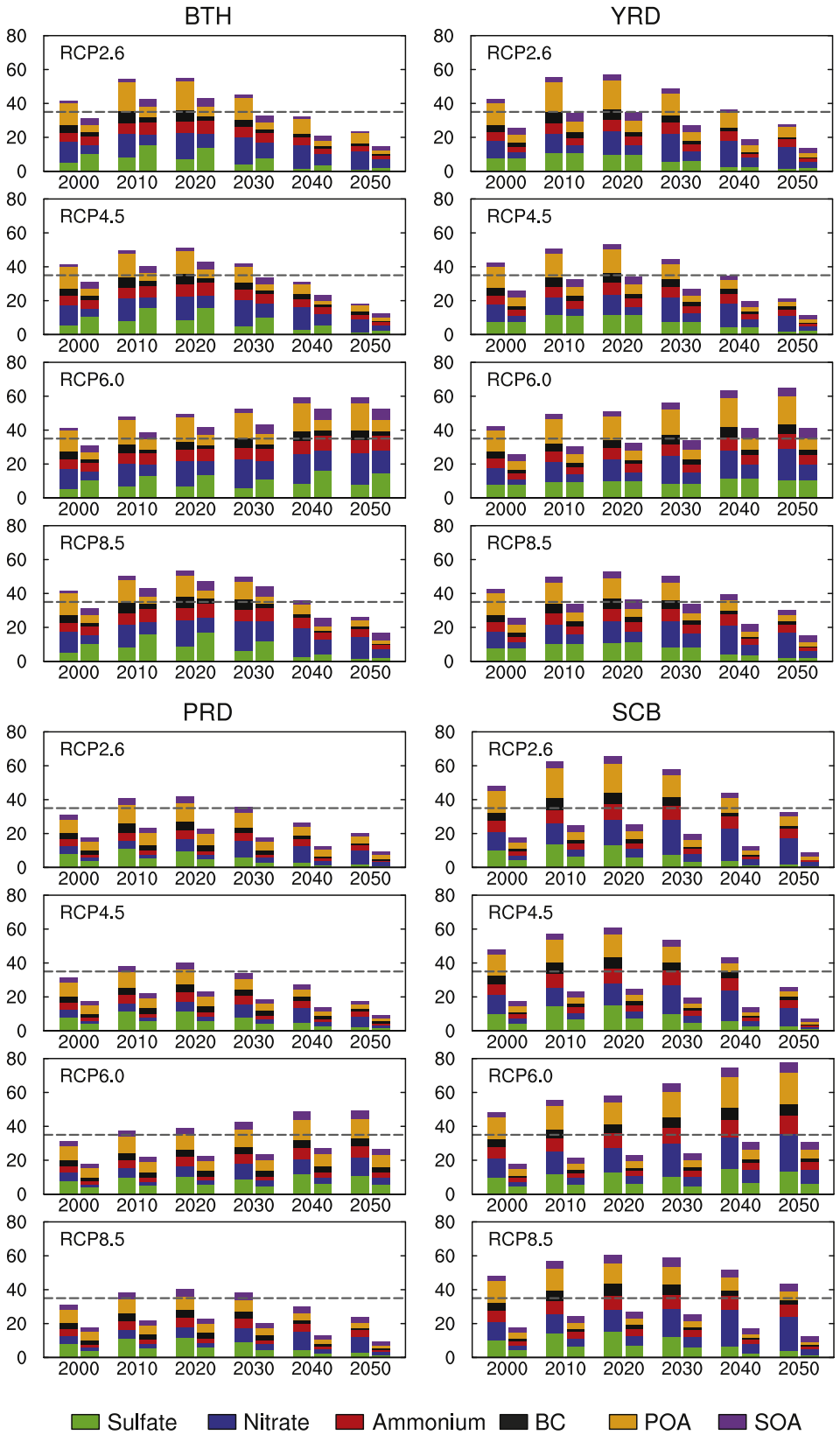

Fig. 11. Predicted $PM_{2.5}$ component concentrations (units: μg m^{-3}) in DJF (left column) and JJA (right column) over BTH, YRD, PRD, and SCB for the period of 2000–2050 under the four RCPs. The dashed line in each plot denotes the baseline of 35 μg m^{-3} in $PM_{2.5}$ concentration suggested by the FGNS.

concentrations up to 60.00 μg m^{-3} are simulated in 2010–2030 under all the RCPs. Wintertime $PM_{2.5}$ concentrations < 35 μg m^{-3} only appear in 2050 under RCP2.6 and RCP4.5.

Notably, over YRD and PRD, the years when $PM_{2.5}$ concentrations meet FGNS in this study are later than those predicted by Li et al. (2016), who modeled $PM_{2.5}$ without SOA. For example, under RCP8.5,

the winter $PM_{2.5}$ over YRD below 35 μg m^{-3} will appear in 2050, instead of 2040 as Li et al. (2016) predicted. Over PRD, the $PM_{2.5}$ was expected to meet FGNS well according to Li et al. (2016). However, in our study the winter $PM_{2.5}$ over PRD exceeds 35 μg m^{-3} in 2010–2020 under RCP2.6 and RCP4.5, and in 2010–2030 under RCP8.5. Moreover, $PM_{2.5}$ pollution in the future atmosphere will be worse if mitigation measures are not taken timely, as implied by RCP6.0.

6.3. Sensitivity of SOA production to future changes in emissions of aromatics and POA

Table 1 shows that the mitigation of POA emission (CTRL_2010_RCP4.5–POA_C2050) over 2010–2050 reduces SOA production and burden over China by 0.17 Tg $year^{-1}$ and 0.0014 Tg, respectively. Future reductions in aromatics (CTRL_2010_RCP4.5–Arom_C2050) reduce SOA production and burden by 0.46 Tg $year^{-1}$ and 0.0052 Tg, respectively. The combined effect of reductions in emissions of both POA and aromatics would lead to a reduction of SOA production by 0.61 Tg $year^{-1}$ and of SOA burden by 0.0064 Tg. These results indicate that reducing the emissions of aromatics, which mainly come from industrial solvent usage and vehicle exhausts, or replacing them with environmentally friendly chemicals is helpful for the future control of SOA pollution (Zhang et al., 2013).

7. Projected SOA DRF over China under the RCPs

The present-day (2010) all-sky DRFs at the TOA relative to pre-industrial times (1850) are calculated to be −0.43 to −0.52 W m^{-2} averaged over the whole of China under the four RCPs (Fig.12). Regionally, the largest negative DRF of exceeding −1.60 W m^{-2} is simulated over the SCB. Table 2 compares our estimated present-day DRF values with those reported in previous studies. The estimated annual mean DRFs of SOA by other models were in a range of −0.01 to −0.41 W m^{-2} on a global mean basis (Hoyle et al., 2009; Lin et al., 2014; Myhre et al., 2013; Spracklen et al., 2011). The global and annual mean DRFs of SOA from our global simulations (4° latitude × 5° longitude) are −0.24 to −0.31 W m^{-2} under the four RCPs, which are within the range obtained from other models. The simulated maximum DRF of −1.60 W m^{-2} over China in our study also agrees closely with the maximum DRFs of −1.00 to −1.50 W m^{-2} over eastern China as presented by other models (Hoyle et al., 2009; Lin et al., 2014).

The projected annual mean all-sky SOA DRFs at the TOA for the period of 2010–2050 relative to 2000 over China under the RCPs are shown in Fig. 13. The evolution pattern of the SOA DRF is opposite to that of SOA concentration (Fig. 6), since SOA exhibits a cooling effect. The negative DRF relative to 2000 averaged over eastern China (20°–45°N, 100°–125°E) peaks in 2020 under RCP2.6 and RCP4.5, and in 2030 under RCP8.5. The maximums are −0.13 W m^{-2}, −0.12 W m^{-2}, and −0.25 W m^{-2} under RCP2.6, RCP4.5, and RCP8.5, respectively. The positive DRF relative to 2000 is the largest over eastern China in 2050 under RCP2.6 (0.19 W m^{-2}) and RCP4.5 (0.12 W m^{-2}), because emissions of POA and aromatics are considerably reduced by then (Fig. 1). Under RCP6.0, the gradually increased anthropogenic emissions lead to a strong negative DRF of −0.28 W m^{-2} over eastern China from 2000 to 2050. Under RCP8.5, the future increases in emissions of aromatics relative to 2000 (Fig. 1) lead to future increases in SOA mass and negative SOA DRFs of −0.13 W m^{-2} to −0.25 W m^{-2} at the TOA in 2010–2050. In 2050, the projected SOA DRFs averaged over eastern China are calculated to be +0.19, +0.12, −0.28, and −0.17 W m^{-2} for RCP2.6, RCP4.5, RCP6.0, and RCP8.5, respectively. These DRFs are comparable in magnitude to the annual and regional mean ozone DRFs over eastern China (18°–45°N, 95°–125°E) of −0.11 to +0.14 W m^{-2} in 2050 relative to 2000 (Zhu and Liao, 2016). Li et al. (2016) reported that the DRFs of $PM_{2.5}$ (exclude SOA) in 2050 relative to 2000 averaged over eastern China (20°–45°N, 100°–125°E) are +1.22, +1.88, −2.73, and +0.66 W m^{-2} under RCP2.6, RCP4.5,

Table 1
The changes of SOA and $PM_{2.5}$ due to the emission mitigation of POA, aromatics, and both of them in China under RCP4.5. All the values are averaged over the whole of China. $PM_{2.5}$ mass concentration is the sum of mass of sulfate, nitrate, ammonium, BC, POA, and SOA.

	CTRL_2010_RCP4.5	POA_C2050	Arom_C2050	POA_Arom_C2050	POA contribution (CTRL_2010_RCP4.5–POA_C2050)	Arom contribution (CTRL_2010_RCP4.5–Arom_C2050)	POA + Arom contribution (CTRL_2010_RCP4.5–POA_Arom_C2050)
SOA production (Tg $year^{-1}$)	2.27	2.10	1.81	1.66	0.17	0.46	0.61
SOA burden (Tg)	0.0405	0.0391	0.0353	0.0341	0.0014	0.0052	0.0064
SOA concentration (μg m^{-3})	1.40	1.24	1.12	0.98	0.16	0.28	0.42
$PM_{2.5}$ concentration (μg m^{-3})	13.39	11.67	13.36	11.50	1.72	0.03	1.89
SOA contribution to $PM_{2.5}$ (%)	12.6	12.5	10.9	11.0	0.1	1.7	1.6

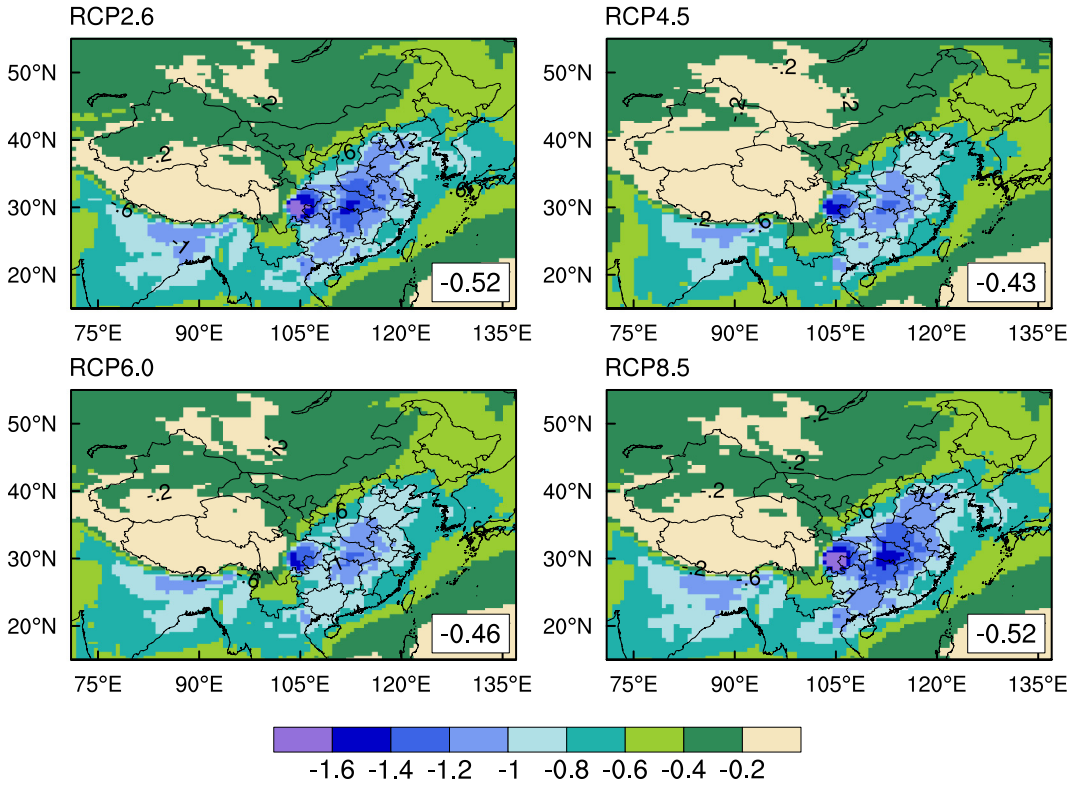

Fig. 12. Simulated annual mean all-sky SOA DRF (units: W m^{-2}) at the TOA for present day (year 2010) relative to preindustrial times (year 1850) under the four RCPs. The DRFs averaged over the whole of China are shown in the bottom-right corner of each panel.

RCP6.0, and RCP8.5, respectively. The inclusion of SOA in $PM_{2.5}$ will enhance the warming (cooling) effects of $PM_{2.5}$ in 2050 under RCP2.6 and RCP4.5 (RCP6.0), but counteract the warming effects in 2050 under RCP8.5.

8. Conclusions

This study applied the nested-grid (0.5° × 0.667°) version of the GEOS-Chem model to simulate future changes (2000–2050) of surface-layer SOA concentrations and the associated DRFs over China in response to future changes in anthropogenic emissions under the four RCPs (RCP2.6, RCP4.5, RCP6.0, and RCP8.5). Comparisons of the simulated present-day (year 2010) SOA concentrations with measurements (year 2012–2013) at 10 sites over China demonstrate that the model can capture reasonably the spatiotemporal distributions of the observed SOA levels (R = 0.62). The model tends to overestimate SOA in JJA with a NMB of 14.2% and underestimate SOA concentrations in other seasons with NMBs in the range of −7.3% to −22.6%.

The projected changes in annual mean SOA concentrations over 2010–2050 generally follow future changes in emissions of toluene and xylene. The largest increase in SOA is found over eastern China in 2020 under RCP2.6 and RCP4.5, in 2050 under RCP6.0, and in 2030 under RCP8.5. Over the four heavily polluted regions, future changes in seasonal mean SOA concentrations exhibit similar trends, but with different magnitudes. Over BTH, the largest changes in SOA concentrations are found in JJA, due to the strongest photochemical reactions in this season. Over YRD, PRD, and SCB, the largest increases are simulated in DJF among all the seasons. The largest increases over YRD (SCB) in DJF are simulated to be 44.3% (39.4%) in 2020, 29.3% (28.3%) in 2020, 116.9% (88.3%) in 2050, and 83.7% (72.1%) in 2030 under RCP2.6, RCP4.5, RCP6.0, and RCP8.5, respectively.

For all RCPs, the contributions of SOA to $PM_{2.5}$ are 3.2–14.3% in DJF, and 10.0–27.0% in JJA over the four regions of BTH, YRD, PRD, and SCB. The contributions of SOA to $PM_{2.5}$ increase with time during 2010–2050 under RCP2.6, RCP4.5, and RCP8.5. Concentrations of SOA are projected to be able to exceed those of sulfate, ammonium, and BC in the future. The earliest time with SOA exceeding sulfate in concentration is simulated to be JJA 2040 over YRD under RCP2.6 and RCP8.5 and over SCB under all the RCPs except RCP6.0. SOA is simulated to exceed ammonium in JJA 2030 over YRD under RCP2.6 and RCP8.5 as well as over SCB under RCP4.5 and RCP8.5. Note that the contributions from biogenic SOA are high in these regions, which account for 24.6–42.7% (32.1–49.8%) in SOA averaged over YRD (SCB) in 2000–2050 under the four RCPs.

The annual mean SOA DRF over eastern China (20°–45°N, 100°–125°E) in 2050 relative to 2000 are simulated to be +0.19 W m^{-2} and + 0.12 W m^{-2}, responding to reductions in SOA over this region

Table 2
Comparisons of the simulated all-sky DRF of SOA at the TOA in this work with the values reported in previous studies.

Reference	Model	Year	Region	DRF (W m^{-2})
Yin et al. (2015)	RegCM4	July 2006	China	−1.12[a]
Jo et al. (2013)	GEOS-Chem	2009	Global	−0.28[a]
O'Donnell et al. (2011)	ECHAM5-HAM	2000	Global	−0.31[a]
Spracklen et al. (2011)	GLOMAP	2000	Global	−0.26 ± 0.15
Lin et al. (2014)	IMPACT	1870–2000	Global	−(0.12–0.31)
Myhre et al. (2013)	6 models	1850–2000 (or 2006)	Global	−(0.01–0.21)
Hoyle et al. (2009)	Oslo CTM2	1750–2004	Global	−(0.06–0.09)
This study	GEOS-Chem	1850–2010	Global	−(0.24–0.31)[b]
			China	−(0.43–0.52)

[a] The values refer to DREs.
[b] The global DRFs are calculated from global (4° latitude × 5° longitude) simulations.

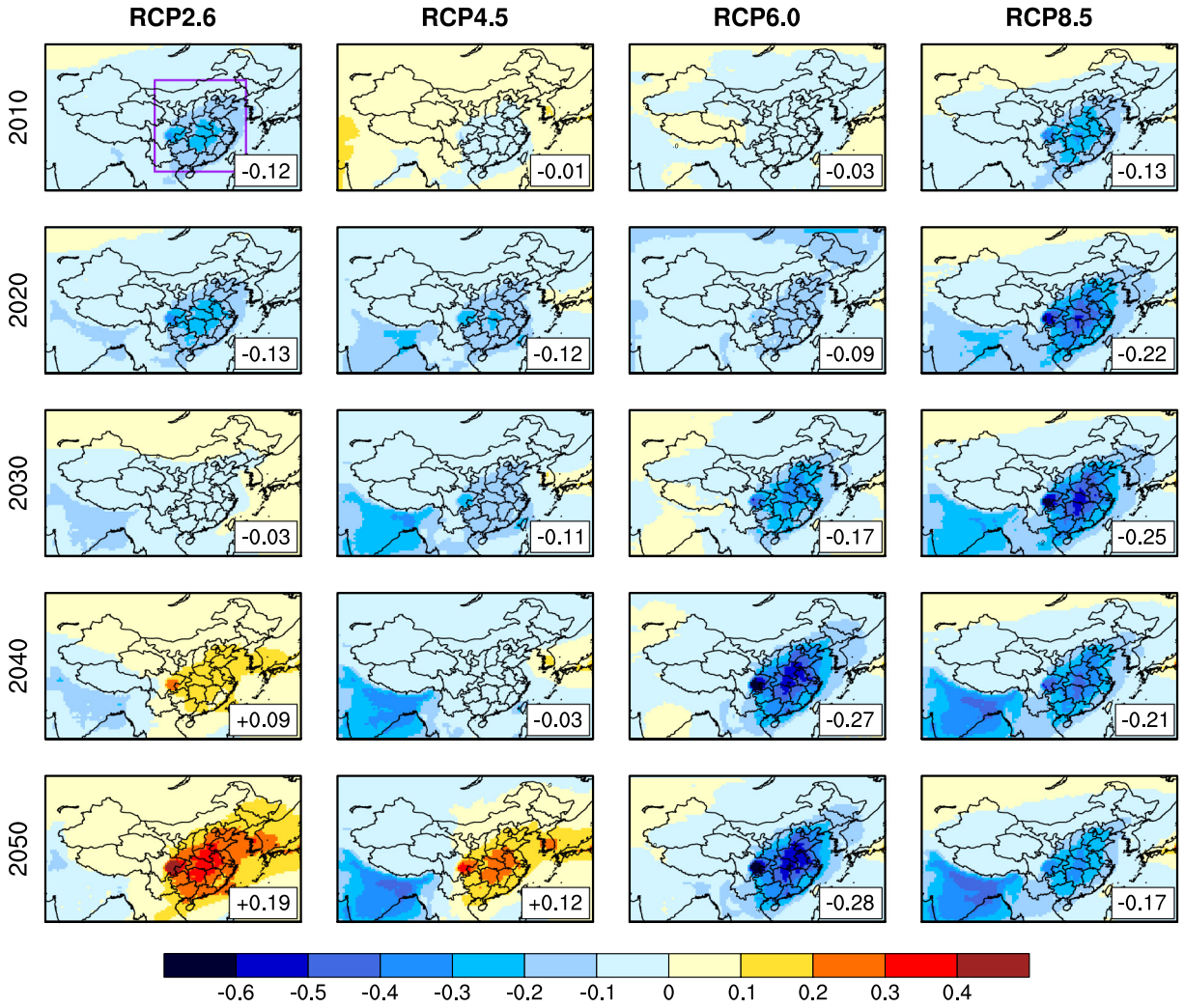

Fig. 13. Predicted changes in annual mean all-sky SOA DRF (units: W m^{-2}) at the TOA in China over 2010–2050 for each decade relative to 2000 under the four RCPs. The DRF averaged over eastern China (20°–45°N, 100°–125°E, see the purple frame in the first panel) is shown in the bottom-right corner of each panel. (For interpretation of the references to color in this figure legend, the reader is referred to the web version of this article.)

under RCP2.6 and RCP4.5, respectively. Although RCP8.5 is a scenario with mitigation, the emissions of toluene and xylene in 2050 are still larger than those in 2000, resulting in an increase in SOA level and a negative DRF of −0.17 W m^{-2} over eastern China. Under RCP6.0, an overall increase of SOA leads to a negative DRF of −0.28 W m^{-2} over eastern China in 2050.

Note that there are some sources of uncertainties in this study. Firstly, our simulation of SOA only accounts for SOA formation from semi-volatile VOCs; we don't consider other pathways like SOA formation from intermedium VOCs or semi-volatile POA (Pye and Seinfeld, 2010), the heterogeneous uptake of dicarbonyls (Fu et al., 2008), and the aqueous reactions in clouds (Lim et al., 2010). Secondly, the optical parameter used for SOA is as same as that of POA, which may induce some bias for SOA DRF (Yin et al., 2015). Thirdly, the impact of future climate change on future SOA levels on an interannual to decadal time scale (Cai et al., 2017; Fu et al., 2016; Liao et al., 2006) is not considered in our study. These are the issues that need to be further studied.

Acknowledgement

This work was supported by the National Basic Research Program of China (973 program, grant 2014CB441202) and the National Natural Science Foundation of China under grants 91744311, 91544219, 41475137, and 41722305.

Appendix A. Supplementary data

Supplementary data to this article can be found online at https://doi.org/10.1016/j.scitotenv.2018.05.274.

References

Alexander, B., Park, R.J., Jacob, D.J., Li, Q.B., Yantosca, R.M., Savarino, J., Lee, C.C.W., Thiemens, M.H., 2005. Sulfate formation in sea-salt aerosols: constraints from oxygen isotopes. J. Geophys. Res.-Atmos. 110. https://doi.org/10.1029/2004jd005659.

Bey, I., Jacob, D.J., Yantosca, R.M., Logan, J.A., Field, B.D., Fiore, A.M., Li, Q.B., Liu, H.G.Y., Mickley, L.J., Schultz, M.G., 2001. Global modeling of tropospheric chemistry with assimilated meteorology: model description and evaluation. J. Geophys. Res.-Atmos. 106:23073–23095. https://doi.org/10.1029/2001jd000807.

Cai, W.J., Li, K., Liao, H., Wang, H.J., Wu, L.X., 2017. Weather conditions conducive to Beijing severe haze more frequent under climate change. Nat. Clim. Chang. 7:257–262. https://doi.org/10.1038/Nclimate3249.

Calvert, J.G., Atkinson, R., Becker, K.H., Kamens, R.M., Seinfeld, J.H., Wallington, T.J., Yarwood, G., 2002. The Mechanisms of Atmospheric Oxidation of the Aromatic Hydrocarbons. Oxford University Press, New York.

Cao, J.J., Lee, S.C., Ho, K.F., Zhang, X.Y., Zou, S.C., Fung, K., Chow, J.C., Watson, J.G., 2003. Characteristics of carbonaceous aerosol in Pearl River Delta Region, China during 2001 winter period. Atmos. Environ. 37:1451–1460. https://doi.org/10.1016/S1352-2310(02)01002-6.

Cao, J.J., Lee, S.C., Ho, K.F., Zou, S.C., Fung, K., Li, Y., Watson, J.G., Chow, J.C., 2004. Spatial and seasonal variations of atmospheric organic carbon and elemental carbon in Pearl River Delta Region, China. Atmos. Environ. 38:4447–4456. https://doi.org/10.1016/j.atmosenv.2004.05.016.

Cao, J.J., Shen, Z.X., Chow, J.C., Watson, J.G., Lee, S.C., Tie, X.X., Ho, K.F., Wang, G.H., Han, Y.M., 2012. Winter and summer PM2.5 chemical compositions in fourteen Chinese cities. J. Air Waste Manage. Assoc. 62:1214–1226. https://doi.org/10.1080/10962247.2012.701193.

Carlton, A.G., Bhave, P.V., Napelenok, S.L., Edney, E.O., Sarwar, G., Pinder, R.W., Pouliot, G.A., Houyoux, M., 2010. Model representation of secondary organic aerosol in CMAQv4.7. Environ. Sci. Technol. 44:8553–8560. https://doi.org/10.1021/es100636q.

Chen, D., Wang, Y., McElroy, M.B., He, K., Yantosca, R.M., Le Sager, P., 2009. Regional CO pollution and export in China simulated by the high-resolution nested-grid GEOS-Chem model. Atmos. Chem. Phys. 9:3825–3839. https://doi.org/10.5194/acp-9-3825-2009.

Colette, A., Bessagnet, B., Vautard, R., Szopa, S., Rao, S., Schucht, S., Klimont, Z., Menut, L., Clain, G., Meleux, F., Curci, G., Rouil, L., 2013. European atmosphere in 2050, a regional air quality and climate perspective under CMIP5 scenarios. Atmos. Chem. Phys. 13:7451–7471. https://doi.org/10.5194/acp-13-7451-2013.

Cooke, W.F., Liousse, C., Cachier, H., Feichter, J., 1999. Construction of a 1 degrees x 1 degrees fossil fuel emission data set for carbonaceous aerosol and implementation and radiative impact in the ECHAM4 model. J. Geophys. Res.-Atmos. 104:22137–22162. https://doi.org/10.1029/1999jd900187.

Ding, X., Wang, X.M., Gao, B., Fu, X.X., He, Q.F., Zhao, X.Y., Yu, J.Z., Zheng, M., 2012. Tracer-based estimation of secondary organic carbon in the Pearl River Delta, south China. J. Geophys. Res.-Atmos. 117:5313. https://doi.org/10.1029/2011jd016596.

Ding, X., He, Q.F., Shen, R.Q., Yu, Q.Q., Wang, X.M., 2014. Spatial distributions of secondary organic aerosols from isoprene, monoterpenes, β-caryophyllene, and aromatics over China during summer. J. Geophys. Res. Atmos. 119:11,877–11,891. https://doi.org/10.1002/2014jd021748.

Ding, X., He, Q.F., Shen, R.Q., Yu, Q.Q., Zhang, Y.Q., Xin, J.Y., Wen, T.X., Wang, X.M., 2016. Spatial and seasonal variations of isoprene secondary organic aerosol in China: significant impact of biomass burning during winter. Sci. Rep. 6:20411. https://doi.org/10.1038/srep20411.

Duan, J.C., Tan, J.H., Cheng, D.X., Bi, X.H., Deng, W.J., Sheng, G.Y., Fu, J.M., Wong, M.H., 2007. Sources and characteristics of carbonaceous aerosol in two largest cities in Pearl River Delta Region, China. Atmos. Environ. 41:2895–2903. https://doi.org/10.1016/j.atmosenv.2006.12.017.

Fairlie, T.D., Jacob, D.J., Park, R.J., 2007. The impact of transpacific transport of mineral dust in the United States. Atmos. Environ. 41:1251–1266. https://doi.org/10.1016/j.atmosenv.2006.09.048.

Farina, S.C., Adams, P.J., Pandis, S.N., 2010. Modeling global secondary organic aerosol formation and processing with the volatility basis set: implications for anthropogenic secondary organic aerosol. J. Geophys. Res.-Atmos. 115. https://doi.org/10.1029/2009jd013046.

Feng, T., Li, G.H., Cao, J.J., Bei, N.F., Shen, Z.X., Zhou, W.J., Liu, S.X., Zhang, T., Wang, Y.C., Huang, R.J., Tie, X.X., Molina, L.T., 2016. Simulations of organic aerosol concentrations during springtime in the Guanzhong Basin, China. Atmos. Chem. Phys. 16:10045–10061. https://doi.org/10.5194/acp-16-10045-2016.

Fu, Y., Liao, H., 2012. Simulation of the interannual variations of biogenic emissions of volatile organic compounds in China: impacts on tropospheric ozone and secondary organic aerosol. Atmos. Environ. 59:170–185. https://doi.org/10.1016/j.atmosenv.2012.05.053.

Fu, T.M., Jacob, D.J., Wittrock, F., Burrows, J.P., Vrekoussis, M., Henze, D.K., 2008. Global budgets of atmospheric glyoxal and methylglyoxal, and implications for formation of secondary organic aerosols. J. Geophys. Res.-Atmos. 113. https://doi.org/10.1029/2007jd009505.

Fu, T.M., Cao, J.J., Zhang, X.Y., Lee, S.C., Zhang, Q., Han, Y.M., Qu, W.J., Han, Z., Zhang, R., Wang, Y.X., Chen, D., Henze, D.K., 2012. Carbonaceous aerosols in China: top-down constraints on primary sources and estimation of secondary contribution. Atmos. Chem. Phys. 12:2725–2746. https://doi.org/10.5194/acp-12-2725-2012.

Fu, Y., Tai, A.P.K., Liao, H., 2016. Impacts of historical climate and land cover changes on fine particulate matter (PM2.5) air quality in East Asia between 1980 and 2010. Atmos. Chem. Phys. 16:10369–10383. https://doi.org/10.5194/acp-16-10369-2016.

Gaschen, A., Lang, D., Kalberer, M., Savi, M., Geiser, T., Gazdhar, A., Lehr, C.M., Bur, M., Dommen, J., Baltensperger, U., Geiser, M., 2010. Cellular responses after exposure of lung cell cultures to secondary organic aerosol particles. Environ. Sci. Technol. 44:1424–1430. https://doi.org/10.1021/es902261m.

Guenther, A., Karl, T., Harley, P., Wiedinmyer, C., Palmer, P.I., Geron, C., 2006. Estimates of global terrestrial isoprene emissions using MEGAN (Model of Emissions of Gases and Aerosols from Nature). Atmos. Chem. Phys. 6:3181–3210. https://doi.org/10.5194/acp-6-3181-2006.

Han, Z.W., Xie, Z.X., Wang, G.H., Zhang, R.J., Tao, J., 2016. Modeling organic aerosols over east China using a volatility basis-set approach with aging mechanism in a regional air quality model. Atmos. Environ. 124:186–198. https://doi.org/10.1016/j.atmosenv.2015.05.045.

Heald, C.L., Henze, D.K., Horowitz, L.W., Feddema, J., Lamarque, J.F., Guenther, A., Hess, P.G., Vitt, F., Seinfeld, J.H., Goldstein, A.H., Fung, I., 2008. Predicted change in global secondary organic aerosol concentrations in response to future climate, emissions, and land use change. J. Geophys. Res.-Atmos. 113. https://doi.org/10.1029/2007jd009092.

Heald, C.L., Ridley, D.A., Kroll, J.H., Barrett, S.R.H., Cady-Pereira, K.E., Alvarado, M.J., Holmes, C.D., 2014. Contrasting the direct radiative effect and direct radiative forcing of aerosols. Atmos. Chem. Phys. 14:5513–5527. https://doi.org/10.5194/acp-14-5513-2014.

Henze, D.K., Seinfeld, J.H., Ng, N.L., Kroll, J.H., Fu, T.M., Jacob, D.J., Heald, C.L., 2008. Global modeling of secondary organic aerosol formation from aromatic hydrocarbons: high-vs. low-yield pathways. Atmos. Chem. Phys. 8:2405–2420. https://doi.org/10.5194/acp-8-2405-2008.

Hoyle, C.R., Myhre, G., Berntsen, T.K., Isaksen, I.S.A., 2009. Anthropogenic influence on SOA and the resulting radiative forcing. Atmos. Chem. Phys. 9:2715–2728. https://doi.org/10.5194/acp-9-2715-2009.

Hu, J.L., Wang, P., Ying, Q., Zhang, H.L., Chen, J.J., Ge, X.L., Li, X.H., Jiang, J.K., Wang, S.X., Zhang, J., Zhao, Y., Zhang, Y.Y., 2017. Modeling biogenic and anthropogenic secondary organic aerosol in China. Atmos. Chem. Phys. 17:77–92. https://doi.org/10.5194/acp-17-77-2017.

Huang, R.J., Zhang, Y., Bozzetti, C., Ho, K.F., Cao, J.J., Han, Y., Daellenbach, K.R., Slowik, J.G., Platt, S.M., Canonaco, F., Zotter, P., Wolf, R., Pieber, S.M., Bruns, E.A., Crippa, M., Ciarelli, G., Piazzalunga, A., Schwikowski, M., Abbaszade, G., Schnelle-Kreis, J., Zimmermann, R., An, Z., Szidat, S., Baltensperger, U., El Haddad, I., Prevot, A.S., 2014. High secondary aerosol contribution to particulate pollution during haze events in China. Nature 514:218–222. https://doi.org/10.1038/nature13774.

Intergovernmental Panel on Climate Change (IPCC), Climate Change 2013. The Physical Science Basis. Contribution of Working Group I to the Fifth Assessment Report of the Intergovernmental Panel on Climate Change. Cambridge Univ. Press, Cambridge, U.K. and New York.

Jathar, S.H., Farina, S.C., Robinson, A.L., Adams, P.J., 2011. The influence of semi-volatile and reactive primary emissions on the abundance and properties of global organic aerosol. Atmos. Chem. Phys. 11:7727–7746. https://doi.org/10.5194/acp-11-7727-2011.

Jiang, F., Liu, Q., Huang, X.X., Wang, T.J., Zhuang, B.L., Xie, M., 2012. Regional modeling of secondary organic aerosol over China using WRF/Chem. J. Aerosol Sci. 43:57–73. https://doi.org/10.1016/j.jaerosci.2011.09.003.

Jo, D.S., Park, R.J., Kim, M.J., Spracklen, D.V., 2013. Effects of chemical aging on global secondary organic aerosol using the volatility basis set approach. Atmos. Environ. 81:230–244. https://doi.org/10.1016/j.atmosenv.2013.08.055.

Lambe, A.T., Cappa, C.D., Massoli, P., Onasch, T.B., Forestieri, S.D., Martin, A.T., Cummings, M.J., Croasdale, D.R., Brune, W.H., Worsnop, D.R., Davidovits, P., 2013. Relationship between oxidation level and optical properties of secondary organic aerosol. Environ. Sci. Technol. 47:6349–6357. https://doi.org/10.1021/es401043j.

Lane, T.E., Donahue, N.M., Pandis, S.N., 2008. Simulating secondary organic aerosol formation using the volatility basis-set approach in a chemical transport model. Atmos. Environ. 42:7439–7451. https://doi.org/10.1016/j.atmosenv.2008.06.026.

Li, K., Liao, H., Zhu, J., Moch, J.M., 2016. Implications of RCP emissions on future PM2.5 air quality and direct radiative forcing over China. J. Geophys. Res.-Atmos. 121:12985–13008. https://doi.org/10.1002/2016JD025623.

Li, J.L., Zhang, M.G., Wu, F.K., Sun, Y.L., Tang, G.G., 2017. Assessment of the impacts of aromatic VOC emissions and yields of SOA on SOA concentrations with the air quality model RAMS-CMAQ. Atmos. Environ. 158:105–115. https://doi.org/10.1016/j.atmosenv.2017.03.035.

Liao, H., Chen, W.T., Seinfeld, J.H., 2006. Role of climate change in global predictions of future tropospheric ozone and aerosols. J. Geophys. Res. Atmos. (1984–2012) 111. https://doi.org/10.1029/2005jd006852.

Liao, H., Henze, D.K., Seinfeld, J.H., Wu, S., Mickley, L.J., 2007. Biogenic secondary organic aerosol over the United States: comparison of climatological simulations with observations. J. Geophys. Res. Atmos. (1984–2012) 112. https://doi.org/10.1029/2006jd007813.

Lim, Y.B., Tan, Y., Perri, M.J., Seitzinger, S.P., Turpin, B.J., 2010. Aqueous chemistry and its role in secondary organic aerosol (SOA) formation. Atmos. Chem. Phys. 10:10521–10539. https://doi.org/10.5194/acp-10-10521-2010.

Lin, P., Hu, M., Deng, Z., Slanina, J., Han, S., Kondo, Y., Takegawa, N., Miyazaki, Y., Zhao, Y., Sugimoto, N., 2009. Seasonal and diurnal variations of organic carbon in PM2.5 in Beijing and the estimation of secondary organic carbon. J. Geophys. Res.-Atmos. 114. https://doi.org/10.1029/2008jd010902.

Lin, G.X., Penner, J.E., Flanner, M.G., Sillman, S., Xu, L., Zhou, C., 2014. Radiative forcing of organic aerosol in the atmosphere and on snow: effects of SOA and brown carbon. J. Geophys. Res.-Atmos. 119:7453–7476. https://doi.org/10.1002/2013JD021186.

Lin, J., An, J., Qu, Y., Chen, Y., Li, Y., Tang, Y.J., Wang, F., Xiang, W.L., 2016a. Local and distant source contributions to secondary organic aerosol in the Beijing urban area in summer. Atmos. Environ. 124:176–185. https://doi.org/10.1016/j.atmosenv.2015.08.098.

Lin, G., Penner, J.E., Zhou, C., 2016b. How will SOA change in the future? Geophys. Res. Lett. 43. https://doi.org/10.1002/2015gl067137.

Liu, H., Jacob, D.J., Bey, I., Yantosca, R.M., 2001. Constraints from 210Pb and 7Be on wet deposition and transport in a global three-dimensional chemical tracer model driven by assimilated meteorological fields. J. Geophys. Res. 106:12109–12128. https://doi.org/10.1029/2000jd900839.

Mari, C., Jacob, D.J., Bechtold, P., 2000. Transport and scavenging of soluble gases in a deep convective cloud. J. Geophys. Res.-Atmos. 105:22255–22267. https://doi.org/10.1029/2000jd900211.

Mauderly, J.L., Chow, J.C., 2008. Health effects of organic aerosols. Inhal. Toxicol. 20:257–288. https://doi.org/10.1080/08958370701866008.

Murphy, B.N., Pandis, S.N., 2009. Simulating the formation of semivolatile primary and secondary organic aerosol in a regional chemical transport model. Environ. Sci. Technol. 43:4722–4728. https://doi.org/10.1021/es803168a.

Murphy, B.N., Pandis, S.N., 2010. Exploring summertime organic aerosol formation in the eastern United States using a regional-scale budget approach and ambient measurements. J. Geophys. Res.-Atmos. 115. https://doi.org/10.1029/2010jd014418.

Myhre, G., Samset, B.H., Schulz, M., Balkanski, Y., Bauer, S., Berntsen, T.K., Bian, H., Bellouin, N., Chin, M., Diehl, T., Easter, R.C., Feichter, J., Ghan, S.J., Hauglustaine, D., Iversen, T., Kinne, S., Kirkevag, A., Lamarque, J.F., Lin, G., Liu, X., Lund, M.T., Luo, G., Ma, X., van Noije, T., Penner, J.E., Rasch, P.J., Ruiz, A., Seland, O., Skeie, R.B., Stier, P., Takemura, T., Tsigaridis, K., Wang, P., Wang, Z., Xu, L., Yu, H., Yu, F., Yoon, J.H., Zhang, K., Zhang, H., Zhou, C., 2013. Radiative forcing of the direct aerosol effect from AeroCom Phase II simulations. Atmos. Chem. Phys. 13:1853–1877. https://doi.org/10.5194/acp-13-1853-2013.

Ng, N., Kroll, J., Chan, A., Chhabra, P., Flagan, R., Seinfeld, J., 2007. Secondary organic aerosol formation from m-xylene, toluene, and benzene. Atmos. Chem. Phys. 7:3909–3922. https://doi.org/10.5194/acpd-7-4085-2007.

O'Donnell, D., Tsigaridis, K., Feichter, J., 2011. Estimating the direct and indirect effects of secondary organic aerosols using ECHAM5-HAM. Atmos. Chem. Phys. 11:8635–8659. https://doi.org/10.5194/acp-11-8635-2011.

Park, R.J., Jacob, D.J., Chin, M., Martin, R.V., 2003. Sources of carbonaceous aerosols over the United States and implications for natural visibility. J. Geophys. Res.-Atmos. 108. https://doi.org/10.1029/2002jd003190.

Park, R.J., Jacob, D.J., Field, B.D., Yantosca, R.M., Chin, M., 2004. Natural and transboundary pollution influences on sulfate-nitrate-ammonium aerosols in the United States: implications for policy. J. Geophys. Res.-Atmos. 109. https://doi.org/10.1029/2003jd004473.

Pye, H.O.T., Seinfeld, J.H., 2010. A global perspective on aerosol from low-volatility organic compounds. Atmos. Chem. Phys. 10:4377–4401. https://doi.org/10.5194/acp-10-4377-2010.

Pye, H.O.T., Liao, H., Wu, S., Mickley, L.J., Jacob, D.J., Henze, D.K., Seinfeld, J.H., 2009. Effect of changes in climate and emissions on future sulfate-nitrate-ammonium aerosol levels in the United States. J. Geophys. Res.-Atmos. 114. https://doi.org/10.1029/2008jd010701.

Rohr, A.C., 2013. The health significance of gas- and particle-phase terpene oxidation products: a review. Environ. Int. 60:145–162. https://doi.org/10.1016/j.envint.2013.08.002.

Spracklen, D.V., Jimenez, J.L., Carslaw, K.S., Worsnop, D.R., Evans, M.J., Mann, G.W., Zhang, Q., Canagaratna, M.R., Allan, J., Coe, H., McFiggans, G., Rap, A., Forster, P., 2011. Aerosol mass spectrometer constraint on the global secondary organic aerosol budget. Atmos. Chem. Phys. 11:12109–12136. https://doi.org/10.5194/acp-11-12109-2011.

Stone, E.A., Zhou, J.B., Snyder, D.C., Rutter, A.P., Mieritz, M., Schauer, J.J., 2009. A comparison of summertime secondary organic aerosol source contributions at contrasting urban locations. Environ. Sci. Technol. 43:3448–3454. https://doi.org/10.1021/es8025209.

Su, M.F., Lin, Y.P., Fan, X.Q., Peng, L., Zhao, C.S., 2012. Impacts of global emissions of CO, NOx, and CH4 on China tropospheric hydroxyl free radicals. Adv. Atmos. Sci. 29: 838–854. https://doi.org/10.1007/s00376-012-1229-2.

Tsigaridis, K., Kanakidou, M., 2003. Global modelling of secondary organic aerosol in the troposphere: a sensitivity analysis. Atmos. Chem. Phys. 3:1849–1869. https://doi.org/10.5194/acp-3-1849-2003.

Tsigaridis, K., Kanakidou, M., 2007. Secondary organic aerosol importance in the future atmosphere. Atmos. Environ. 41:4682–4692. https://doi.org/10.1016/j.atmosenv.2007.03.045.

Volkamer, R., Klotz, B., Barnes, I., Imamura, T., Wirtz, K., Washida, N., Becker, K.H., Platt, U., 2002. OH-initiated oxidation of benzene - part I. Phenol formation under atmospheric conditions. Phys. Chem. Chem. Phys. 4:1598–1610. https://doi.org/10.1039/b108747a.

Wang, Y., Zhang, X., Sun, J., Zhang, X., Che, H., Li, Y., 2015. Spatial and temporal variations of the concentrations of PM 10, PM 2.5 and PM 1 in China. Atmos. Chem. Phys. 15: 13585–13598. https://doi.org/10.5194/acpd-15-15319-2015.

Weber, R.J., Sullivan, A.P., Peltier, R.E., Russell, A., Yan, B., Zheng, M., De Gouw, J., Warneke, C., Brock, C., Holloway, J.S., 2007. A study of secondary organic aerosol formation in the anthropogenic-influenced southeastern United States. J. Geophys. Res. Atmos. (1984–2012) 112. https://doi.org/10.1029/2007jd008408.

Wesely, M.L., 1989. Parameterization of surface resistances to gaseous dry deposition in regional-scale numerical-models. Atmos. Environ. 23:1293–1304. https://doi.org/10.1016/0004-6981(89)90153-4.

Wiedinmyer, C., Tie, X., Guenther, A., Neilson, R., Granier, C., 2006. Future changes in biogenic isoprene emissions: how might they affect regional and global atmospheric chemistry? Earth Interact. 10:101–111. https://doi.org/10.1175/EI174.1.

Yang, L.X., Zhou, X.H., Wang, Z., Zhou, Y., Cheng, S.H., Xu, P.J., Gao, X.M., Nie, W., Wang, X.F., Wang, W.X., 2012. Airborne fine particulate pollution in Jinan, China: concentrations, chemical compositions and influence on visibility impairment. Atmos. Environ. 55:506–514. https://doi.org/10.1016/j.atmosenv.2012.02.029.

Yin, C.Q., Wang, T.J., Solmon, F., Mallet, M., Jiang, F., Li, S., Zhuang, B.L., 2015. Assessment of direct radiative forcing due to secondary organic aerosol over China with a regional climate model. Tellus B 67. https://doi.org/10.3402/Tellusb.V67.24634.

Zhang, X., Wang, Y., Niu, T., Zhang, X., Gong, S., Zhang, Y., Sun, J., 2012. Atmospheric aerosol compositions in China: spatial/temporal variability, chemical signature, regional haze distribution and comparisons with global aerosols. Atmos. Chem. Phys. 12: 779–799. https://doi.org/10.5194/acp-12-779-2012.

Zhang, Y., Wang, X., Barletta, B., Simpson, I.J., Blake, D.R., Fu, X., Zhang, Z., He, Q., Liu, T., Zhao, X., Ding, X., 2013. Source attributions of hazardous aromatic hydrocarbons in urban, suburban and rural areas in the Pearl River Delta (PRD) region. J. Hazard. Mater. 250-251:403–411. https://doi.org/10.1016/j.jhazmat.2013.02.023.

Zhao, C., Wang, Y.H., Yang, Q., Fu, R., Cunnold, D., Choi, Y., 2010. Impact of East Asian summer monsoon on the air quality over China: view from space. J. Geophys. Res.-Atmos. 115. https://doi.org/10.1029/2009jd012745.

Zhu, J., Liao, H., 2016. Future ozone air quality and radiative forcing over China owing to future changes in emissions under the Representative Concentration Pathways (RCPs). J. Geophys. Res. Atmos. 121:1978–2001. https://doi.org/10.1002/2015jd023926.